AD-780 504

IR WINDOW STUDIES

Ferdinand A. Kroger, et al

University of Southern California

Prepared for:

Air Force Cambridge Research Laboratories
Defense Advanced Research Projects Agency

15 September 1973

UNCLASSIFIED

Security Classification

AD 780 504

DOCUMENT CONTROL DATA - R & D

(Security classification of title, body of abstract and indexing annotation must be entered when the overall report is classified)

1. ORIGINATING ACTIVITY (Corporate author) University of Southern California Electronic Sciences Laboratory Los Angeles, California 90007	2a. REPORT SECURITY CLASSIFICATION UNCLASSIFIED 2b. GROUP

3. REPORT TITLE

IR WINDOW STUDIES

4. DESCRIPTIVE NOTES (Type of report and inclusive dates)

Scientific Interim.

5. AUTHOR(S) (First name, middle initial, last name)

Ferdinand Kroger
John H. Marburger

6. REPORT DATE	7a. TOTAL NO. OF PAGES	7b. NO. OF REFS
15 September 1973	74	10

8a. CONTRACT OR GRANT NO.	9a. ORIGINATOR'S REPORT NUMBER(S)
F1968-72-C-0275 ✓ b. PROJECT, Task, Work Unit Nos. 2055 n/a n/a c. DoD Element 61101D d. DoD Subelement n/a	Quarterly Technical Report No. 5 ✓ 9b. OTHER REPORT NO(S) (Any other numbers that may be assigned this report) AFCRL-TR-73-0680

10. DISTRIBUTION STATEMENT

A-Approved for public release; distribution unlimited

11. SUPPLEMENTARY NOTES	12. SPONSORING MILITARY ACTIVITY
This research was supported by the Defence Advanced Research Projects Agency.	Air Force Cambridge Research Laboratories (LQ) L. G. Hanscom Field Bedford, Massachusetts 01730

13. ABSTRACT

The temperature dependence of the 10μ absorption of GaAs in air shows contributions by free carriers above 250°C, and surface effects due to oxidation. The dielectric constant of GaAs is found to be 12.4 ± 0.12. An accurate method to determine the oxygen content of GaAs has been developed. Results obtained so far give 10^{17} - $10^{18}cm^{-3}$ or 6×10^{14} O atoms per cm^2 surface. Conditions favorable to the growth of thick layer GaAs have been established. Pure KCl has $K \approx 10^{-4}cm^{-1}$. KBr has been purified and crystals have been grown. Absorption measurements are hindered by surface reactions. Analysis of the defect structure of CdTe was completed, and the parameters of the constants of defect formation reactions and defect diffusion were obtained. Experimental conditions leading to high resistivity, stoichiometric material were established. Hot pressing of CdTe was started. A surface wave technique of measuring small k's was further developed. The fundamental processes underlying multiphonon absorption were further investigated. Applicability of the L-S-T relation to GaAs was checked. A caustic surface analysis for thermal lensing was made, and the stress and the stress fields in non-uniformly stresses windows were determined.

77

DD FORM 1 NOV 65 1473 (PAGE 1)

0102-014-6600

UNCLASSIFIED

Security Classification

14 KEY WORDS	LINK A		LINK B		LINK C	
	ROLE	WT	ROLE	WT	ROLE	WT
IR Windows						
Alkali Halides						
III-V Semiconductors						
II-VI Semiconductors						
Thermal lensing						
IR absorption						

ia

ARPA Order No. 2055

Program Code No. 3D10

Contractor: University of Southern California

Effective Date of Contract 1 June 1972

Contract No. F19628-72-C-0275

Principal Investigator and Phone No.
Prof. John H. Marburger/213 746-2227/9
Prof. F. A. Kroger/213 746-6224
AFCRL Project Scientist and Phone No.
Alfred Kahan/617 861-4014

Contract Expiration Date 30 Nov. 1973

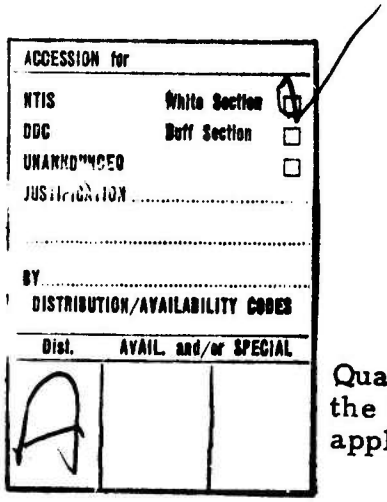

Qualified requestors may obtain additional copies from the Defense Documentation Center. All others should apply to the National Technical Information Service.

ABSTRACT

Three films of GaAs, 10-30 μm thick, have been grown by liquid epitaxy at 800°C. A method was developed to measure the oxygen content in liquid gallium. Using this method, the oxygen content of two GaAs samples was determined and was found to be 10^{17} and 10^{18} O cm^{-3}. Should this be present at the surface, it would correspond to 6×10^{14} atoms O cm^{-2}. The conditions to grow bulk GaAs by chemical vapor transport were established. KCl and KCl-OH crystals previously grown proved to have $k_{10.6\,\mu} \approx 10^{-4}$ cm^{-1}; however, the results are not reliable due to T fluctuations and/or surface absorption. KBr crystals have been grown from purified materials. Reaction with the atmosphere has prevented reliable absorption measurements.

The first experiments of hot pressing CdTe in the presence of liquid Cd have been done. The excess Cd escaped too early for it to help reach the required densification. Stress-strain tests were carried out on Si-doped GaAs in air between 250 and 550°C. Strain hardening is observed to an extent increasing with decreasing length/width ratio.

Capacitance and conductance changes upon biasing a metal GaAs·Cr contact are attributed to the presence of deep Cr levels. The dielectric constant was found to be 12.4 ± 0.12. Analysis of self diffusion and high-temperature Hall effect data on pure and indium doped CdTe have yielded a complete defect model, parameters for the constants of various defect formation reactions, and expressions for the diffusion constants of various defects as f(T). Conditions for obtaining high-resistivity CdTe have been established. Investigations of the possible effect of electric moment per volume and local ionic displacements multi-phonon absorption have continued.

The Lyddane-Sachs-Teller relation seems to be obeyed by GaAs at room temperature, but not at lower temperatures. An increase of absorption coefficient at 9.5 μ at T > 250°C is due partly to free carrier formation, partly to irreversible surface damage (oxidation). A method of measurement of low absorption coefficients and temporal thermal expansion from surface absorption of a light pulse using acoustic surface waves is further developed. For non-piezo electric surfaces (KCl) coupling is achieved by a fluid layer. A caustic surface analysis for thermal lensing was made, and the stress fields in non-uniformly stressed windows were analyzed.

CONTENTS

1. INTRODUCTION

The format of this report follows closely that of the first quarterly report in which projects are identified by codes keyed to the contract work statement.

The various categories are briefly:

a) Crystal growth
b) Polycrystalline window fabrication
c) Mechanical properties of window materials
d) Window material defect characterization
e) Theory of residual IR optical absorption
f) Absorption measurement techniques
g) Theoretical evaluation of optical performances of windows

a. 1 Effect of Oxygen and Other Impurities on IR Absorption in II-VI and III-V Compounds

J. M. Whelan and P. S. Vijayakumar

Liquid Phase Epitaxial Growth of GaAs Films

The horizontal liquid phase epitaxial growth apparatus has been completed. It utilizes a carbon boat containing the Ga solution, the bottom of which can be contacted with a GaAs saturation wafer and then by a GaAs substrate wafer. Both wafers are supported in recesses on a carbon slider. This unit is operated in a H_2 atmosphere which was electrolytically generated and diffused through a Pd-Ag membrane. Temperature is controlled to within $0.03^{\circ}C$ under steady state conditions.

Three trial films have been grown at $\sim 800^{\circ}C$ using cooling rates of $0.06^{\circ}C\ min^{-1}$ on [311] oriented substrates which had dislocation densities under $2000\ cm^{-2}$. Thicknesses of the films were 12, 10 and 29 μm respectively. Large areas of the films are smooth and featureless, although each had a region which was rough. These corresponded to incomplete wiping of the Ga growth solution at the end of the cooling interval. Evidence of surface deterioration of the substrate wafers prior to growth was evident. This may be due to outgassing of the carbon parts which is considered to be the most likely cause. If so, the condition will improve with use. Other possibilities are the presence of H_2O in the H_2 and inadequate cleaning of the seeds during the chemical polishing and final etch-rinse sequence. The former will be checked by monitoring the H_2O content of the exit H_2 with a stabilized zirconia electrolytic concentration cell. This is being assembled at present. Inadequate substrate etching is considered to be unlikely because the same procedures used in this work were adequate for the maintenance of good quality surfaces at $700^{\circ}C$ for several hour long periods. It may be necessary to equilibrate the H_2 with As_4 vapor in approximate equilibrium with GaAs at $800^{\circ}C$.

During the next period the apparatus will be used to grow unintentionally doped layers for their evaluation and with respect to deep level defects.

Studies of Oxygen in GaAs

As has been described earlier, the use of zirconia concentration cells for determining the concentration of oxygen in GaAs is based on measuring the

oxygen fugacity in a suitable metal solvent for the GaAs before and after it is dissolved. Prerequisite information is the relationship between the oxygen fugacities and concentrations in the metal solvent. We have chosen Ga as the initial solvent for study. The procedure for determining the fugacity-concentration relationship is to pump oxygen electrolytically into the Ga metal and measure the cell emf change after allowing time for mixing and after making the oxygen gain-loss corrections as described in the previous report. One gets the change in fugacities corresponding to given additions of oxygen starting with an arbitrary (low) oxygen concentration. Assuming Henry's law to be valid one can extrapolate the results to zero oxygen fugacity with the confidence that the concentration also goes to zero.

Such results are shown in Fig. 1 for a Ga solution at 600°C. The fugacity of dissolved oxygen should be proportional to the square root of the effective molecular oxygen pressure in equilibrium with Ga near the zirconia surface. This effective oxygen pressure p_{O_2} is determined from the cell emf and the oxygen reference pressure at the other electrode. This reference pressure, $p_{O_2 ref}$ is obtained by using a H_2O-H_2 reference gas mixture in contact with that reference electrode. As can be seen in Fig. 1 the changes in fugacity of dissolved oxygen with amount of oxygen are in accord with the dissolved oxygen species containing one atom of oxygen and that species seems to obey Henry's law. At the lower oxygen concentrations, i.e., below mol fractions of 1.2×10^{-7}, an apparent deviation in Henry's law is suggested. This is an artifact associated with significant deviations of the cell emf's from their reversible values.

Using the data shown in Fig. 1 the oxygen concentration in two GaAs samples was estimated by measuring the time dependence of the oxygen fugacity in the Ga near the cell wall before and after dissolving GaAs in the solution. The long term drift rates of these fugacities are extrapolated to the time the GaAs was dissolved and the change related to the change in oxygen content of the Ga. Differences in oxygen concentrations upon dissolving samples GaAs-1 and GaAs-2 correspond to approximately 10^{18} and 10^{17} oxygen atoms cm^{-3} if the possibility of surface oxide is excluded. If all the oxygen in the latter sample is attributed to surface oxygen, its surface concentration would correspond to about 6×10^{14} oxygen atoms cm^{-2}.

Use of this method will be continued using GaAs samples with low absorption coefficients in the 10 μm region. One recognizable limitation to this method is that it will be not detected if the Ga solution or GaAs sample contains a "getter" for the oxygen. One such agent may well be Si. Its effect will also be investigated.

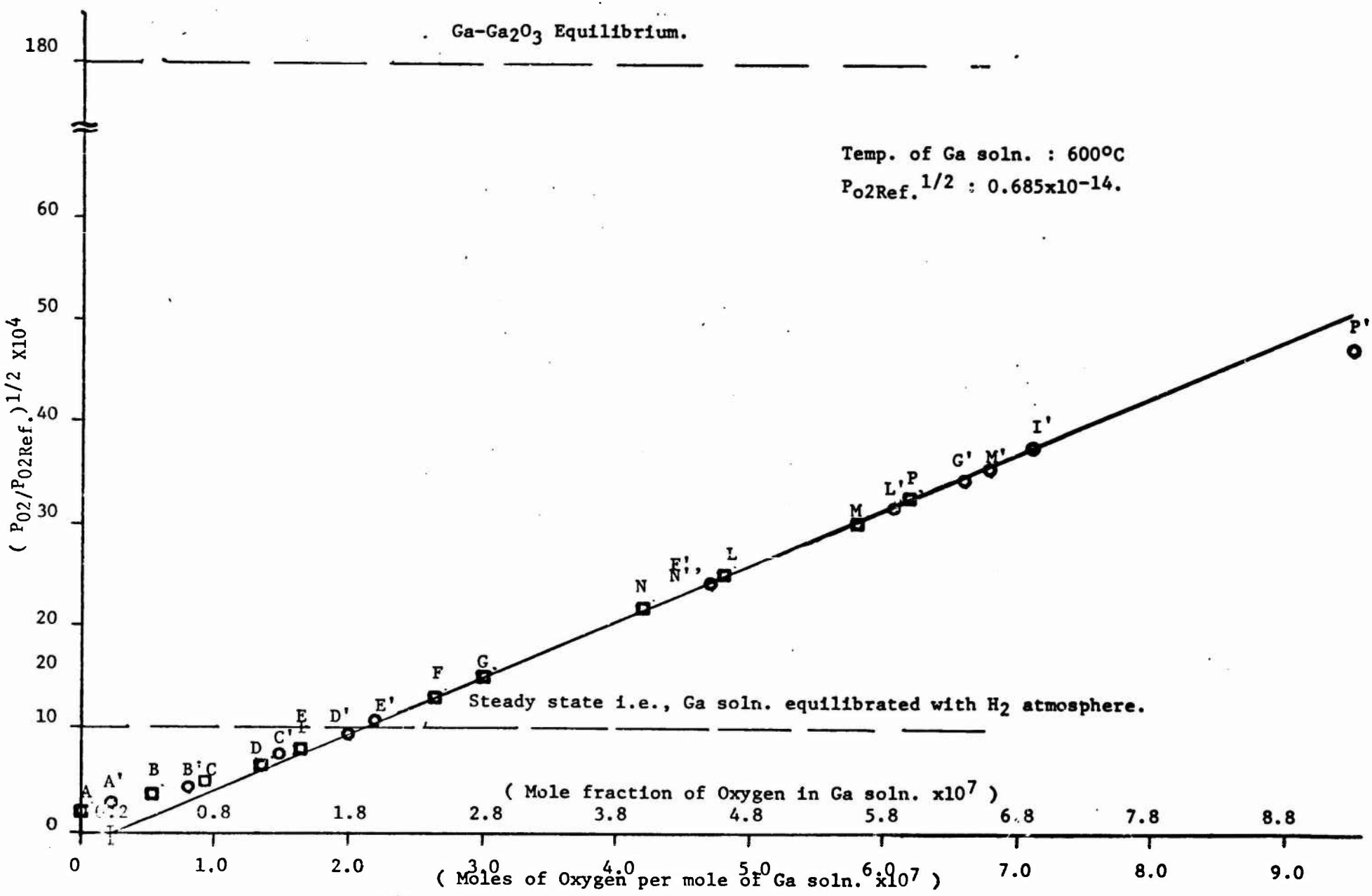

Changes in $(P_{O2}/P_{O2Ref.})^{1/2}$ associated with additions of Oxygen to the Ga soln. Changes are represented by unprime to corresponding prime letters.

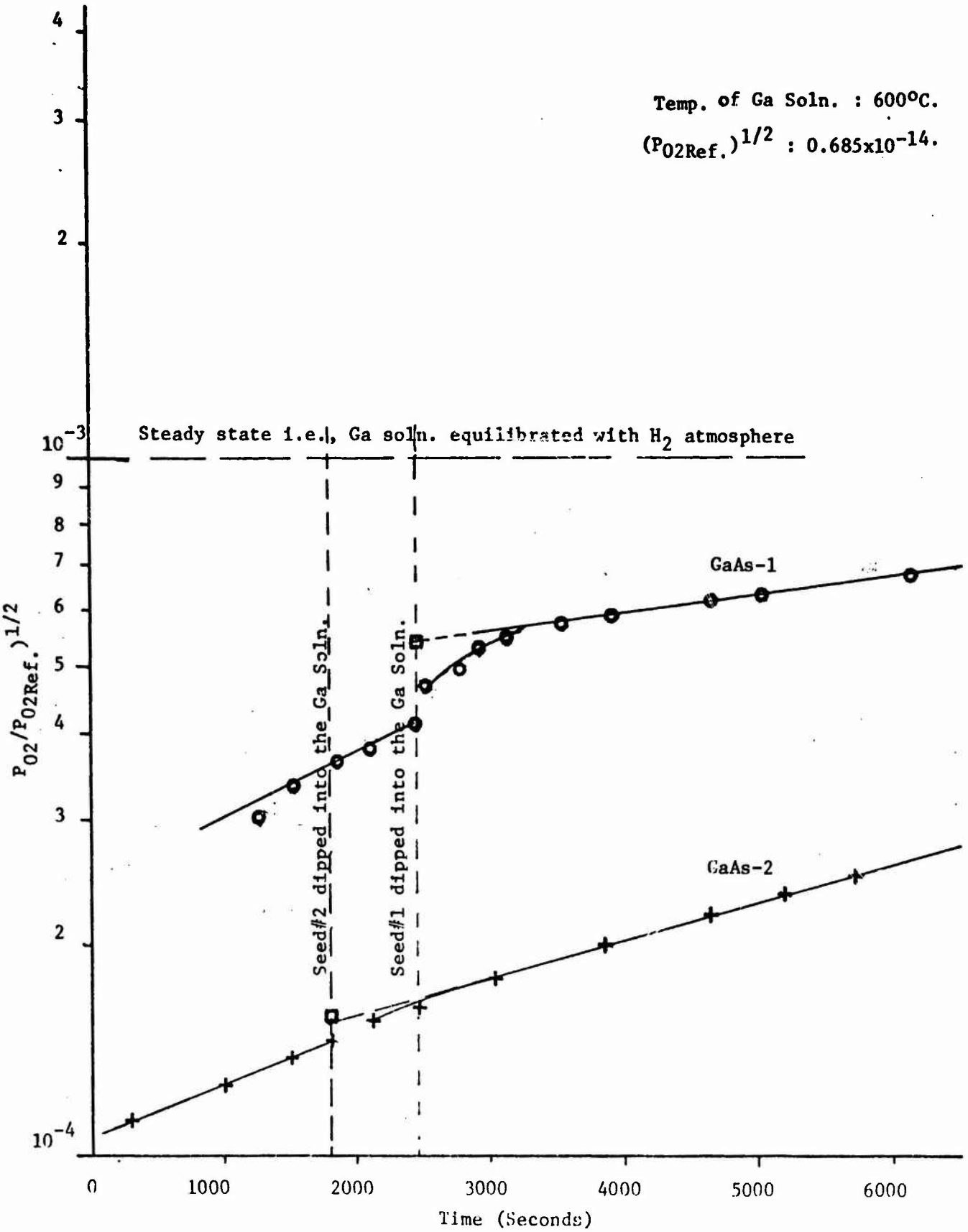

Changes in $(P_{02}/P_{02Ref.})^{1/2}$ upon dissolving GaAs Samples.

a.2 Optimization of Alkali Halide Window Materials

Paul J. Shlichta, Robert E. Chaney

Summary

The 10.6μ absorptions of KCl and KCl:OH crystals were measured by laser calorimetry. The results indicate that the bulk absorptivity is, in both cases, in the 10^{-4} cm^{-1} region but that the measurements are unreliable because of (a) temperature fluctuations during sample heating and cooling, probably due to air convection and/or surface irregularities, and (b) excessive surface absorption. Attempts have been made to minimize the latter problem by developing a new polishing technique, involving the seepage of solvent through a porous polyethylene disk, and by modifying the crystal puller so as to be able to produce crystals with as-grown optical surfaces.

KBr has been purified by ion exchange, fractional crystallization, and treatment with HBr and Br_2 and single crystals have been grown. Attempts to measure the optical absorption of these crystals have been hindered by the excessive tendency of cleaved and polished KBr surfaces to react with the atmosphere.

Sample Preparation and Characterization

Crystal 3-7 was pulled in inert atmosphere from a melt which had been purified by ion exchange, fractional crystallization, and treatment with HCl and Cl_2; these procedures have been described in previous reports. Five samples were cleaved from this crystal. Three (A, B, and C) were mechanically polished, to remove cleavage steps, with 600 grit abrasive paper, then with a Linde A-ethanol slurry on a glass plate, then chemically polished for 30 seconds in a 50% hydrochloric acid solution, and finally rinsed with 95% ethanol. The resulting surfaces were clear and flat but had an "orange peel" texture. The other two specimens (D and E) had stepless cleavage surfaces and were used without further preparation. Ultraviolet spectrophotometry showed no absorption bands in the 2000 - Å region, thereby confirming the absence of detectable concentrations

(1 to 10 mole p.p.m) of heavy-metal cations such as Tl, Pb, Sn, and In, and of anions such as OH^-, O_2^-, $O^=$, and F^-. These samples are regarded as our best effort to date at growing ultrapure KCl crystals.

The hydroxide-doped crystal 4-7,8 was grown from a purified KCl melt to which approximately 0.5 mole % KOH (reagent grade) was added just prior to attempts to pull a crystal. This melt gave off fumes which rapidly attacked the silica growth chamber thereby so greatly impairing visibility as to make pulling impossible. The melt was therefore crystallized by slow cooling. The resultant ingot, when cleaved, yielded two specimens with clear step-free faces in two directions. These samples (A and B) were each measured in two different <100> orientations. Ultraviolet spectrophotometry disclosed a strong absorption peak at 2040 Å, which, according to previous work[1], corresponds to an OH^- concentration of 1.8×10^{-4} mole %. This low value, and the aforementioned rapid attack of the silica growth chamber, suggest that most of the KOH was lost by evaporation; the absence of any other ultraviolet absorption bands precludes any appreciable decomposition of the KOH into K_2O or peroxide.

Calorimetry

The 10.6μ absorption coefficient (β) of the above specimens was measured by laser calorimetry according to the method of Deutsch and Rudko[2]. Because of multiple internal reflections

$$\beta = \frac{1}{\text{path length}} \cdot \frac{\text{power absorbed}}{\text{power transmitted}} \cdot \left(\frac{2n}{1 + n^2} \right) \qquad \text{(a.2.1)}$$

where n is the index of refraction. If the laser beam power is measured by noting the rate of temperature rise of a total-absorption cone beam-stop, then β may be derived from the relation

$$\beta = \frac{1}{L} \cdot \frac{c_s m_s}{c_c m_c} \cdot \frac{2n}{1 + n^2} \cdot \frac{(dT/dt)_s}{(dT/dt)_c} \qquad \text{(a.2.2)}$$

where L is the path length through the specimen, c_s and c_c the specific heats of the specimen and cone, m_s and m_c the masses of the specimen and cone, and $(dT/dt)_s$ and $(dT/dt)_c$ the adiabatic steady-state rates of temperature

rise for specimen and cone when exposed to the laser beam. The adiabatic heating rates may be estimated by subtracting the rate of cooling with the beam off from the rate of heating when the beam is on, i.e.

$$(dT/dt)_s \simeq (dT/dt)_{hs} - (dT/dt)_{cs} \qquad (a.2.3)$$

these quantities are assumed to be linear, as shown in Figure a.2 1.

The observed β is assumed to be the sum of contributions from both bulk and surface absorption; hence the relation

$$B = \beta L = \alpha L + \sigma S \qquad (a.2.4)$$

where α is the true bulk absorptivity, σ is the surface absorption per surface, and S is the number of surfaces through which the beam passes. Therefore, if a series of measurements is made on specimens of varying thickness, but of identical bulk composition and surface condition, a graphic plot of βL versus L will give, by extrapolation to $L = 0$, a value for σS and therefore an estimate of α. This is illustrated in Figures a.2.2 and a.2.3.

The results of the most recent series of measurements are listed in Table a.2.1; it will be noted that the precision is very poor. If we assume that the α of pure KCl (crystal 3-7) is constant from one specimen to another, there are only two likely sources of error: (a) inaccuracies in the heating and cooling curves and (b) variations in σ due to differences in surface preparation. The irregularities in the heating and cooling curves in Figure a.2.1 and the scatter in repeated measurements of the same sample (e.g., crystal 3-7, sample B) indicate that (a) is an important factor and that it is probably caused by air currents around the specimen. The construction of an evacuated sample chamber is therefore being considered. On the other hand, the variations caused by repositioning the specimen and the high σ observed for polished (as opposed to cleaved) surfaces suggest that (b) is also an important factor. For this reason, efforts have been made to develop a new non-abrasive polishing technique (see below). It will be noted, however, that, at least for pure KCl, cleaved surfaces have a far lower σ than polished surfaces. Presumably, as-grown surfaces would be the best

TABLE a.2.1 CALORIMETRIC MEASUREMENTS OF 10.6μ ABSORPTION

Crystal	Specimen	Surface Preparation	L (cm)	$\beta(cm^{-1})$	βL	Average βL
KCl (3-7)	A	polished	0.677	.00239	.00162	
				.00203	.00137	.00153
				.00238	.00161	
	B	polished	1.563	.00115	.00180	
				.00041	.00064	
				.00148	.00231	
				*.00095	*.00148	
				.00167	.00261	
				*.00136	*.00213	
				.00125	.00195	.00184
				.00175	.00274	
				.00098	.00153	
				.00129	.00202	
				.00110	.00171	
				*.00106	*.00165	
				.00090	.00141	
	C	polished	0.612	.00208	.00127	
				.00249	.00152	.00164
				.00282	.00173	
				.00335	.00205	
	D	cleaved	0.575	.00040	.00023	
				.00040	.00023	.00021
				.00034	.00020	
				.00033	.00019	
	E	cleaved	0.217	.00075	.00016	
				.00132	.00029	.00024
				.00124	.00027	
KCl:OH (4-7,8)	$A_{a\ axis}$	cleaved	0.825	.00304	.00251	
				.00319	.00263	.00248
				.00278	.00229	
	$A_{c\ axis}$	cleaved	0.471	.00664	.00313	
				.00574	.00271	
				.00627	.00296	.00285
				*.00598	*.00282	
				.00572	.00270	
				.00591	.00279	
	$B_{a\ axis}$	cleaved	0.818	.00511	.00418	.00383
				.00426	.00349	
	$B_{b\ axis}$	cleaved	0.558	.00398	.00222	
				.00429	.00240	.00221
				.00359	.00200	

* denotes repositioning of specimen

and therefore we have renewed our efforts to grow crystals with optically flat faces.

Despite their poor precision, the measurements reported herein do indicate that, in confirmation of Haas' report[3] and the Raytheon extrapolation[4], the α for pure KCl is below .0002 cm^{-1}. The data for KCl:OH (crystal 4-7,8) does tend to suggest a slight increase in α with [OH], but is at present too inaccurate to merit comment.

Polishing Techniques

The work of Davisson[5] suggests that our mechanical-chemical polishing technique could be greatly improved by annealing the specimen before the final chemical polish. It appears preferable, however, to eliminate mechanical polishing altogether by using a controlled-contour chemical polishing technique, in which specimen would be exposed to a continuously-replenished planar thin film of solvent. One such technique, involving the centrifugal spreading of a solvent film on a rotating glass disk, has already been developed[6]; however, since the necessary apparatus appears to be rather elaborate, alternative easier techniques are being tried first. For example, the apparatus shown schematically in Figure a.2.4 consists merely of a porous polyethylene plate with an appropriate chemical polishing solution slowly seeping through it. The excess solution flows over the side of the plate housing and is collected in an overflow pan. In a series of preliminary experiments, crystals were etched in a $Cu(NO_3)_2$-methanol solution, to produce a rough surface, and then pourous-plate polished sequentially with water, methanol, and ethanol. The resultant surface is approximately planar and smoother than surfaces produced by our previous mechanical-chemical technique.

Crystal-Puller Modifications

Although in previous work with NaCl[7], it was shown that crystals could be pulled from melt with flat faces approaching optical quality, attempts to grow similar crystals of KCl have thus far been unsuccessful. We have finally concluded that this is because of insufficient heat flow through the crystal and up the pull rod. Replacement of the solid silica-

glass pull rod with a copper rod enclosed in a silica tube has resulted in a noticeable but still insufficient improvement. Attempts are now being made to improve the thermal contact between the seed crystal and pull rod.

Efforts to solve another problem --- visibility --- have resulted in the construction of a transparent furnace using a shielded wire heating coil and a gold film radiation reflector (developed by T.B.Reed, Lincoln Laboratories, M.I.T.). This furnace has been constructed and will be tested during the next quarter.

KBr Crystals

During the early part of this quarter, additional ion exchange columns were installed and converted to the K^+ (cationic) and Br^- (anionic) form. The gas manifold was modified to accomodate HBr and Br_2, the latter by bubbling He through a bromine-filled bubbler. KBr was then purified by the same sequence of procedures described previously for KCl. Thus far , two crystals of undoped KBr have been grown.

Specimens were cleaved and mounted for calorimetry but their surfaces were observed to fog and become cloudy within a few minutes of being mounted in the calorimeter. (It should be noted that the calorimeter room is considerably more humid than the specimen preparation area.) The cause of this surface-atmosphere reaction has not yet been established.

References

(1) T. I. Gie and M. V. Klein, Bull. Amer. Phys. Soc., Ser. II, 8 (1963) 230.

(2) T. F. Deutsch and R. I. Rudko, Conference on High Power Infrared Laser Window Materials: October 30, 31 and November 1, 1972, Vol. 1, AFCRL-TR-73-0372(1) (19 June 1973) 201-222.

(3) M. Haas (Naval Research Laboratory), private communication.

4. F. A. Horrigan and T. F. Deutsch, Raytheon Research Division Quarterly Technical Report No. 1, ARPA Order No. 1180, January 1972.

5. J. W. Davisson, Conference on High Power Infrared Laser Window Materials: October 30, 31 and November 1, 1972, Vol. 2, AFCRL-TR-73-0372(2) (19 June 1973) 525-534.

6. L. D. Dyer, Rev. Scient. Inst. (1963) 34, 1114-1116.

7. P. J. Shlichta, Jet Propulsion Laboratory Space Program Summary No. 35-15 Vol. IV (June30, 1962) 88-90.

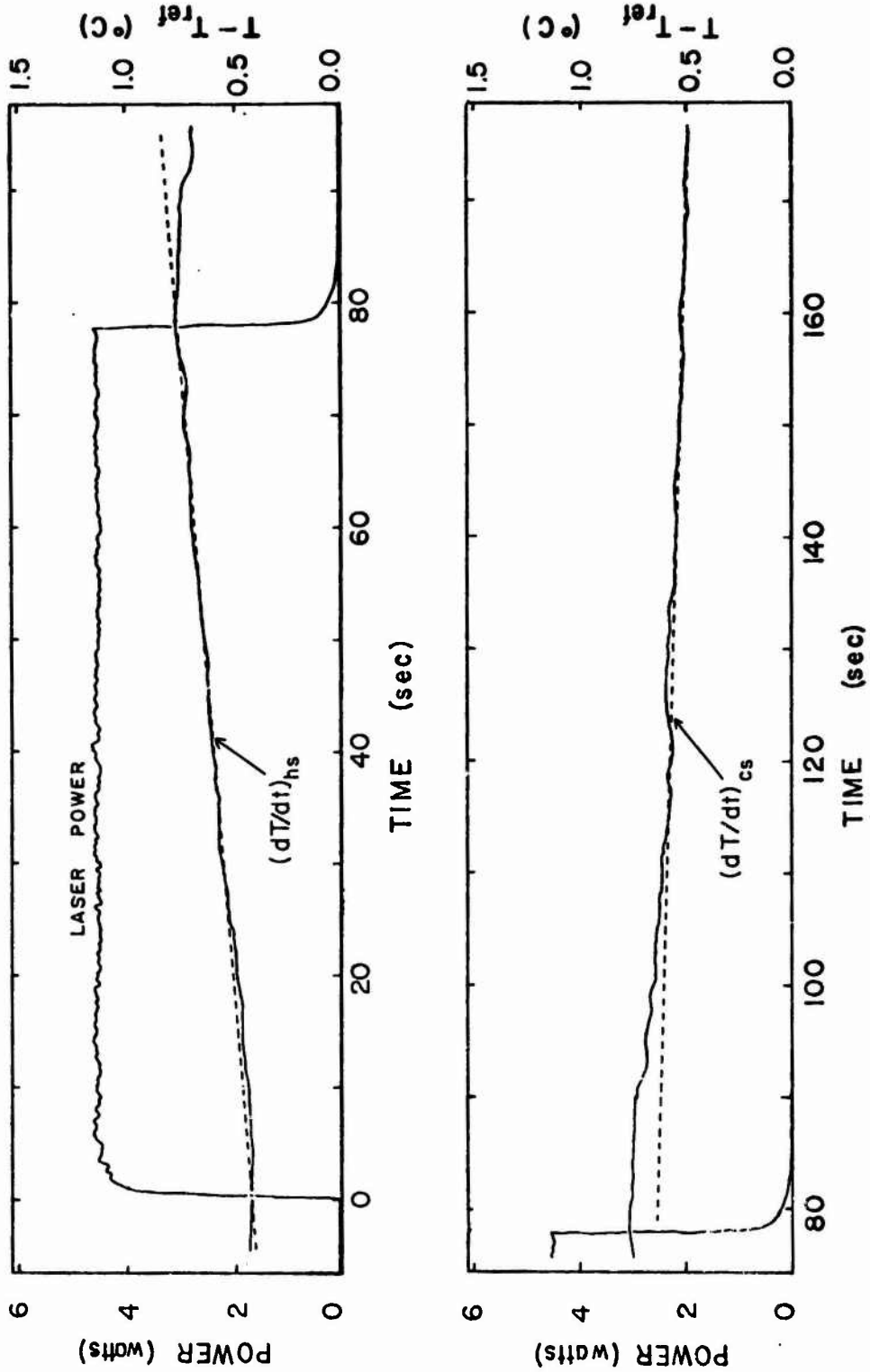

Fig. a.2.1 Typical Heating and Cooling Curves for Calorimetry. Crystal 3-7 Sample B.

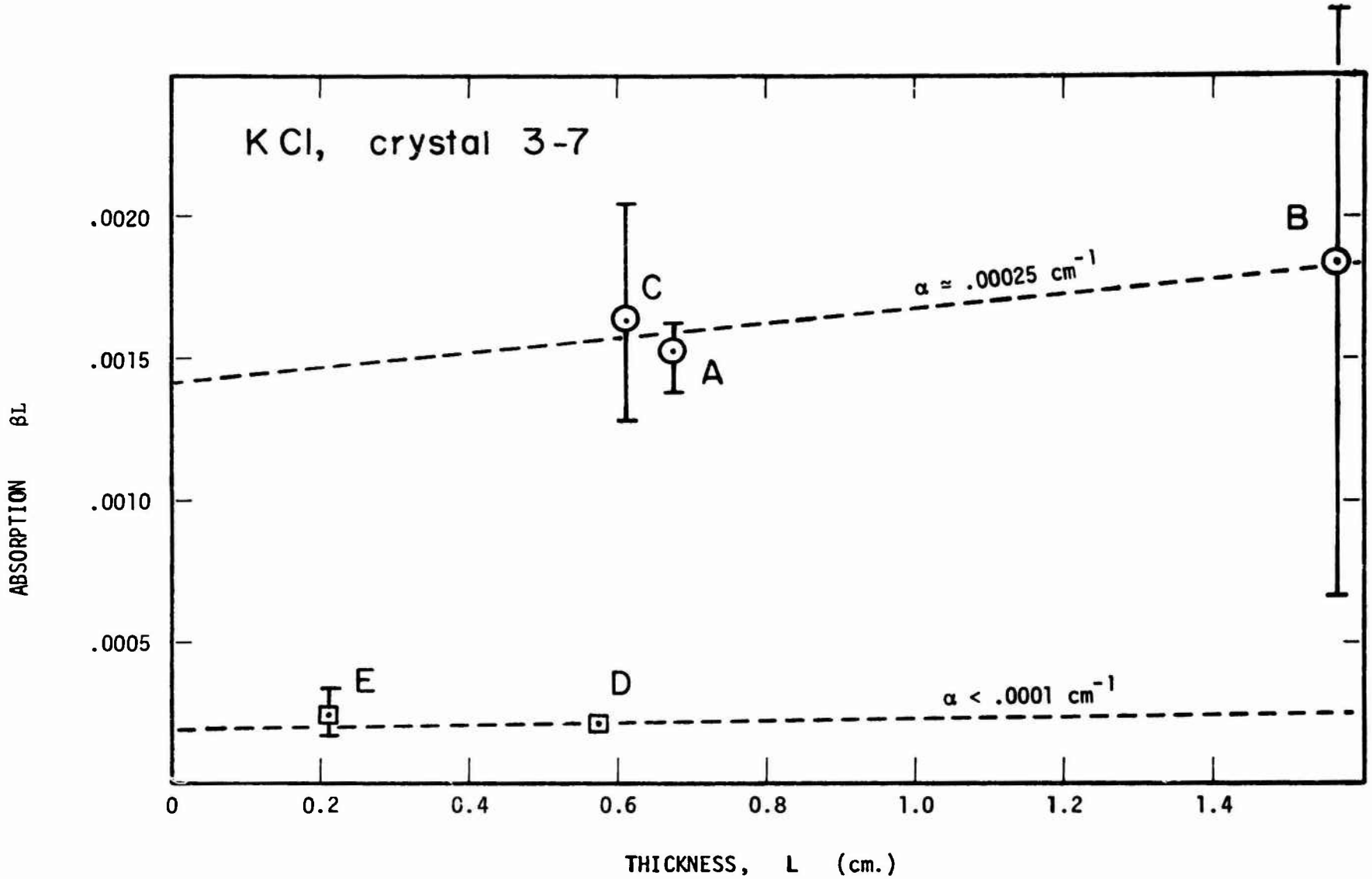

Fig. a.2.2 Calorimetry data for pure KCl(Crystal 3-7). Samples A, B and C polished. Samples D and E cleaved only. Bars indicate extreme values. Circles indicate average.

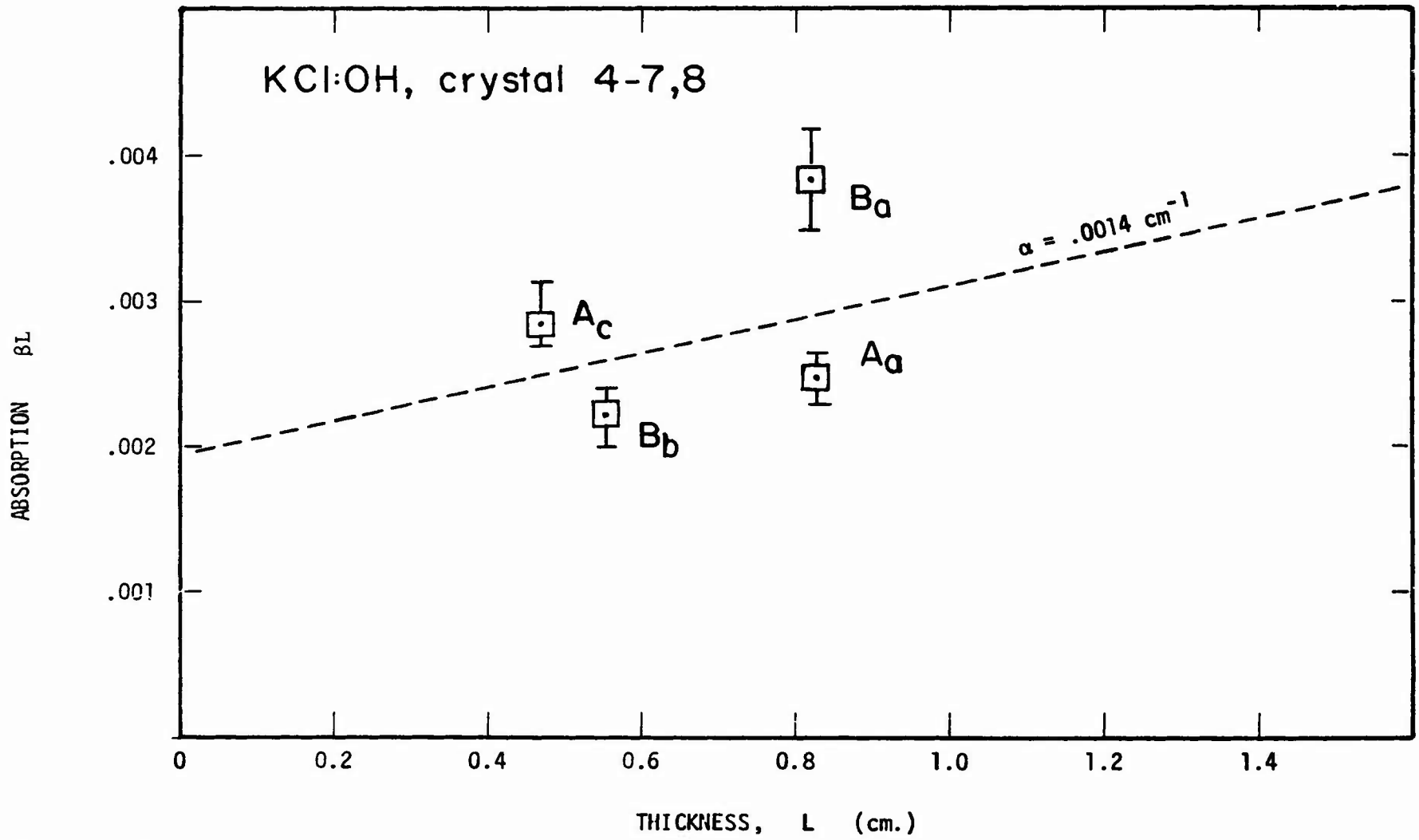

Fig. a.2.3 Calorimetry data for KCl:OH (Crystal 4-7, 8). Bars indicate extreme values. Circles indicate average.

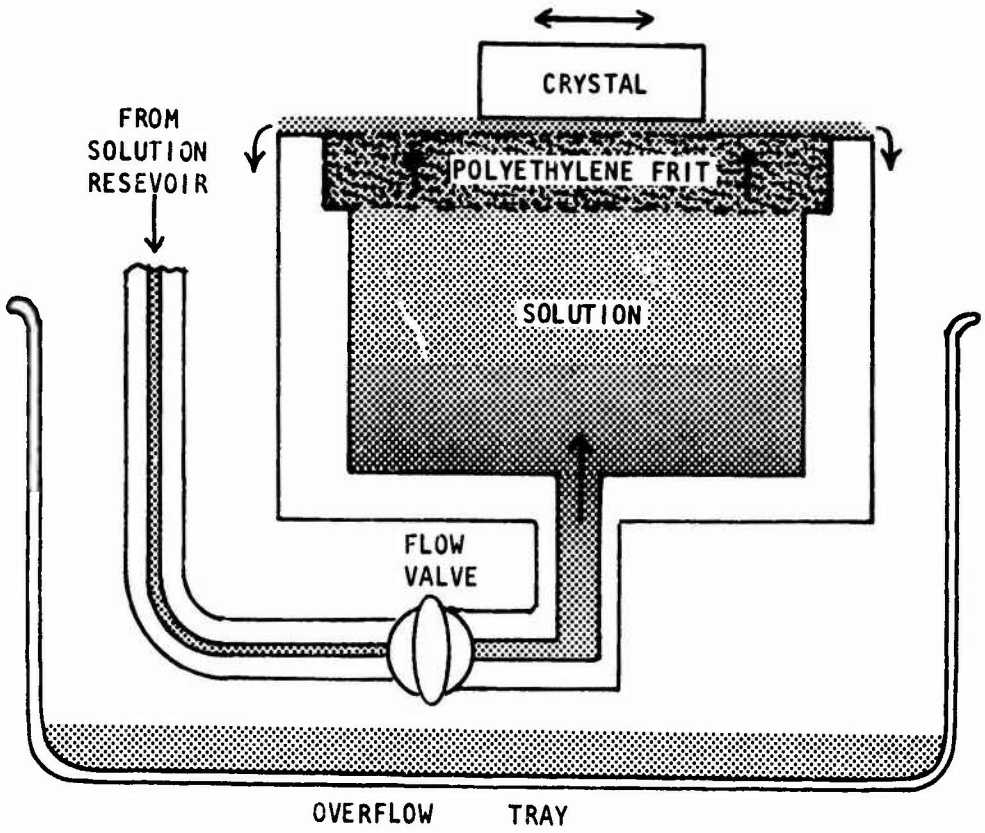

Fig. a.2.4 Schematic Diagram of Apparatus for Controlled-Contour Chemical Polishing Technique.

a.3 Growth of Crystals for IR Window Materials

E. A. Miller and W. R. Wilcox

Work in this period consisted of establishing deposition conditions for bulk growth of GaAs. A modified substrate holder covering a range of 30°C and holding 4 substrates up to 1.5 x 1.5 cm each was constructed. Five runs with deposition times up to 8 days were completed. From these results we were able to determine deposition condictions that should yield bulk GaAs. We also scaled up the Ga boat and the $AsCl_3$ bubbler to contain enough material for a 30 day run. A 30 day run whereby we should obtain bulk samples was started at the close of this reporting period.

Experimental Results and Discussion:

A. Conditions favorable to growth of thin film epitaxial layers are not suitable for long term bulk film growth. For example dendritic overgrowths, if given enough time, can consume reactants from the gas stream near the substrate and even produce etching of the substrate. We attempted to alleviate this by reducing the $AsCl_3$ vapor content by reducing the H_2 flow through the $AsCl_3$ bubbler. This was immediately successful and now, with the low flow rates used, dendritic of needle growth only appears on the tube walls. A verbal communication* also revealed that it may be possible to eliminate wall deposition completely if the $AsCl_3$ vapor content is lowered and the substrate temperture increased sufficiently.

B. Results of CVD #20 deserve special attention. A leak that developed downstream at the exit tube may have been responsible for the unusual faceted growth shown in Figure 1. From a back reflection Laue photograph we determined that the large facet was a (110). Since growth on this facet was very smooth we predicted that epitaxial growth on a (110) substrate may be quite smooth, level, and free of large surgace defects. We currently have two {110} oriented substrates in the 30 day run.

C. Growth on the (111)A substrates (CVD #21, for example) results in a pyramidal form leaving much less surface area at the top, as shown in Fig. 1. This could pose a problem in obtaining a sample for IR absorption measurement

*D. W. Shaw, Texas Instruments, Inc.

Figure 1 Run CVD #20 showing large facets. Magnification 6 x .

in as much as the sample should be as thick on the outside edge as in the middle. We also have two large 1.5 x 1.5 cm (111)A oriented substrates in our 30 day run. This should leave a 1 mm thick x 8-9 mm diameter sample for measurements.

D. Hall measurements on 2 of the larger needles from CVD #18 yielded a value of $n = 8 \times 10^{16}$ cm^{-3}. This indicates improvement must be made in system cleanliness.

E. Currently we have a 30 day deposition run in progress on 2 (110) and 2 (111)A substrates oriented to within 0.5^{o}. Orientation was accomplished by aligning the crystal on our laser goniometer(this apparatus was constructed on a previous ARPA contract). Substrate orientation was further checked with back reflection Laue photographs.

Fugure Work:

A. Obtain thick sample for IR absorption measurements.

B. Obtain Hall data on some of the actual deposited layers.

C. Attempt to improve system cleanliness.

Summary of GaAs CVD Runs 6-1-73 to 8-31-73

Total flow rate: 240 cc/min
Substrate Temperature range: 730-760°C
Substrates: (111)A and (100)

run #	H_2 flow through $AsCl_3$	length of run	major change to system	result
CVD #18	120 cc/min	5 days	long multiple substrate holder	on (111)A substrates dendritic growth; some smooth growth at 750-760°C
CVD #19	60 cc/min	3 days	$AsCl_3$ concentration reduced	on (111)A substrates dendritic growth minimized; growth on surface was quite uniform but more rough.
CVD #20	60 cc/min	3 days	accidental leak downstream	on (111)A substrates faceted growth; large growth pits
CVD #21	50 cc/min	9 days	longer run, reduction of $AsCl_3$ concentration	on (111)A substrate 1 mm thick deposit in one region, large growth pits. on (100) substrate smoother uniform growth, many hillocks, 0.5 mm thick deposit; no dendritic growth on substrates, only on tube walls.

b. 1. Fabrication of Polycrystalline IR Window Materials

S. M. Copley, J. M. Whelan and V. Rana

The goal of this part of the program is to produce samples of laser window materials in polycrystalline form by a novel hot pressing technique involving the use of volatile liquid sintering aids. A detailed description of this technique has been given in previous quarterly reports. Initial experiments are being carried out on CdTe.

CdTe powder, 99.999 pct pure, was obtained from Research Organic/Inorganics.* The powder was prepared by precipitation from solution. Several proprietary purification steps were employed by RO/I to obtain the specified purity. The particle size is sub-micron. In applying our technique to this material, a charge of 5 gms. of powder is loaded into a graphite die along with 2 wt pct Cd (Cd shot with purity of 99.9999 pct**). This is sufficient material to yield a specimen 1/2 in diameter x 1/4 in. thick. An appropriate amount of tin (99.99 pct pure) is loaded in the recess at the top of the die to provide a liquid seal, see Fig. 1(a). The die is then placed in the furnace inside the hot pressing chamber and the chamber is evacuated to a pressure of 30 microns or better. Pressure ranging from 300 to 3000 psi are applied to the die plunger at room temperature and are maintained while the temperature is raised at a rate of approximately $2^{o}C$/min to the final desired temperature. After soaking for a period of time, the pressure is released and the temperature is lowered.

In the initial experiments, it has not been possible to retain the excess Cd in the compacts. Cd loss from the compacts occurs by transport through the vapor phase. Figures 2 and 3 show the microstructures of compacts pressed at $390^{o}C$ and $600^{o}C$, respectively. Although the specimens differ in grain size and degree of sintering, neither have any Cd at

---

*Research Organic/Inorganic Chemical Corpn., Sun Valley Calif.
**Cominco American Incorporated, Spokane, Washington

the three grain junctions. Examination of the die after pressing has shown that the material is effusing from the compact by way of the bottom plunger and condensing at the bottom of the die chamber. The Sn seal appears to be working and we have no evidence for loss from the die chamber. To solve this problem we have redesigned our die as shown in Fig. 1(b). This die can be placed in the furnace so that the compact is the coldest region with which the vapor phase is in contact. It is anticipated that with this design evaporation will be suppressed.

Further experiments are planned with the new die design using both Cd and Te as volatile liquid sintering aids.

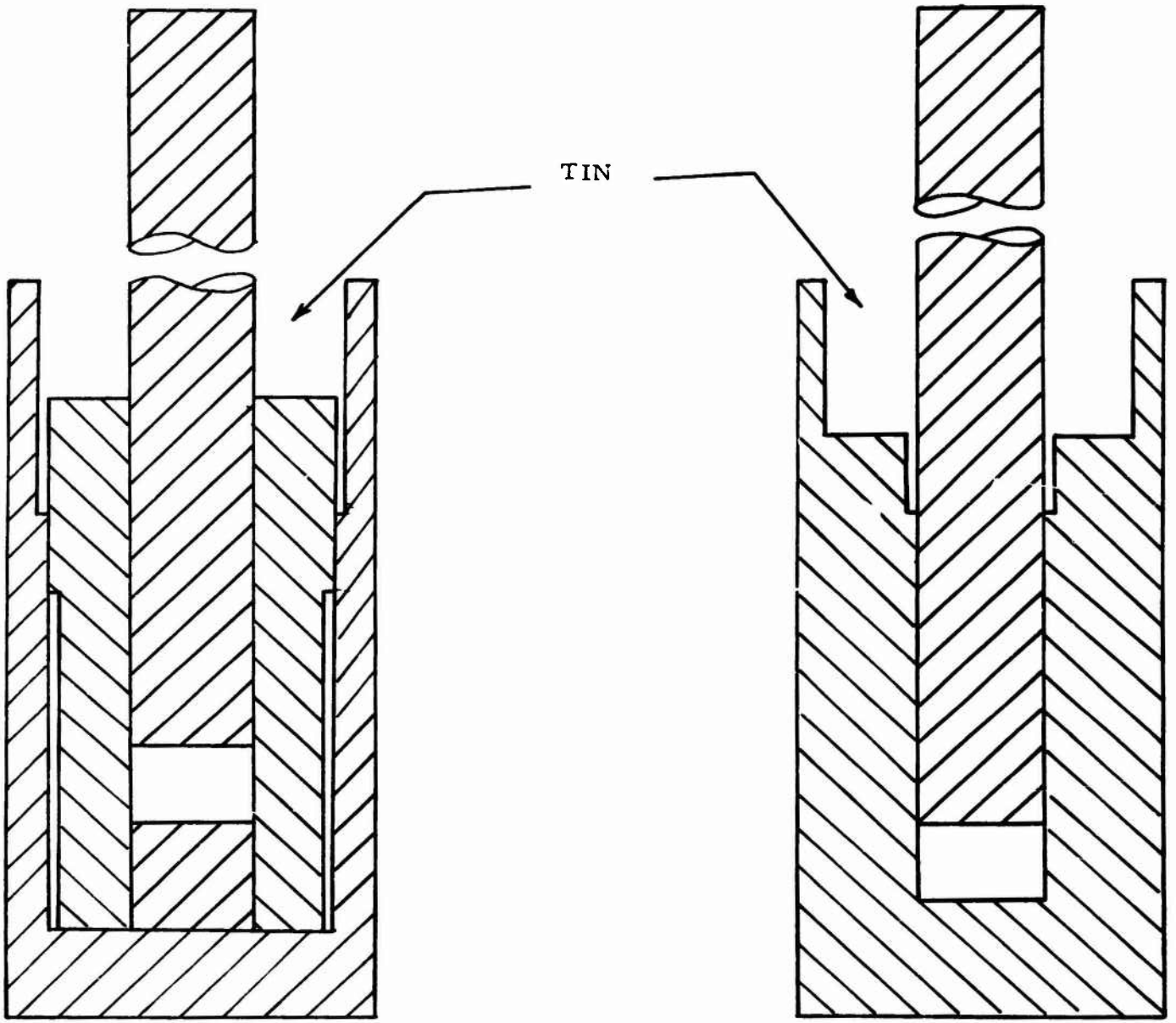

1. Die Assemblies for the hot press

2. Fracture surface of the compact pressed at 300 psi and heated to 390°C, showing the fine grain size and the cavities formed by evaporation of material to the cooler parts of the die.

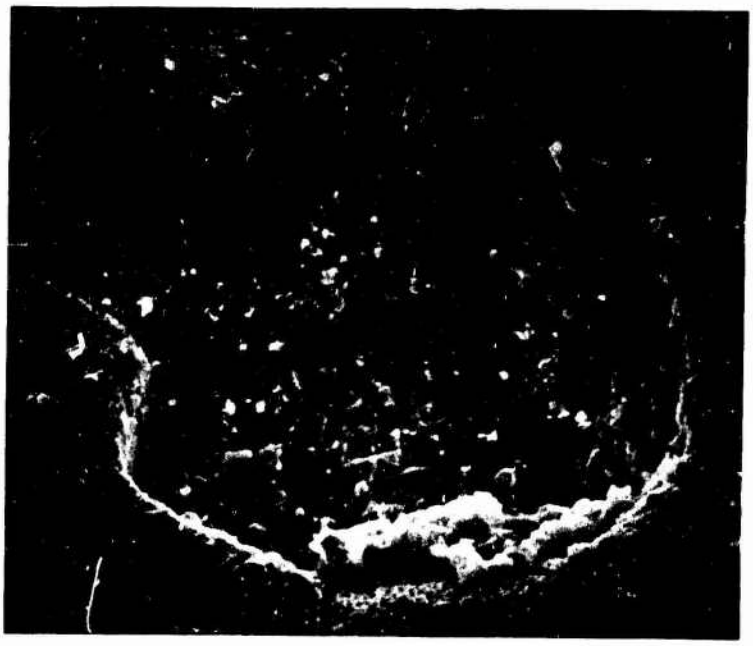

3. Microstructure of the compact pressed at 300 psi and heated to 600°C, showing the grain growth and loss of cadmium that had been confined to three grain junctions at the end of the run.

c. 1 Mechanical Behavior of III-V and II-VI Compounds

S. M. Copley and V. Swaminathan

In this report we will give the summary of the stress-strain experiments that we have been doing on single crystals of silicon doped gallium arsenide.

Experimental Details:

Compression samples were prepared from a melt grown single crystal with a carrier concentration of $10^{18}/cm^3$. Samples having (100) and (111) orientations were prepared with a goniometer and a precision cut-off wheel. They were mechanically polished using 600 grit silicon carbide powder and then chemically polished in a slowly stirred solution of $5H_2SO_4$ - $1H_2O_2$ - $1H_2O$ at 50^oC. Specimens with cross section 0.2 in x 0.2 in and different lengths were obtained.

The specimens were loaded at a constant force rate in a CGS-Lawrence Testing machine. The force rate was adjusted to give an essentially constant stress rate of 20 psi/sec for the first few percent strain. The specimen strain was computed from the loading ram displacement. All stress-strain tests were conducted in air over the entire range of test temperatures (250^oC to 550^oC). The temperature was controlled by a thermocouple placed in contact with the specimen.

Results:

Figure 1 shows the variation of yield stress with temperature for the orientations (111) and (100) obtained by a repeated yielding experiment on samples having length/width ratio as 1.0. Figure 2 and Figure 3 show the stress-strain curves for (100) and (111) orientations at three different temperatures. A linear work hardening region is clearly noticeable in both the figures. Figure 3 also indicates that the strain hardening coefficient is temperature dependent. Figures 4 and 5 indicate the effect of length/width ratio on the stress-strain curves. It is evident that the strain hardening coefficient increases with decreasing length/width ratio in both orientations.

Further experiments to clarify the stress-strain behavior of GaAs single crystals are planned. Slip offset observations will be employed along with yield stress data to reveal the operation of secondary slip systems. Experiments on Cr-doped GaAs (Bell and Howell) will also be carried out.

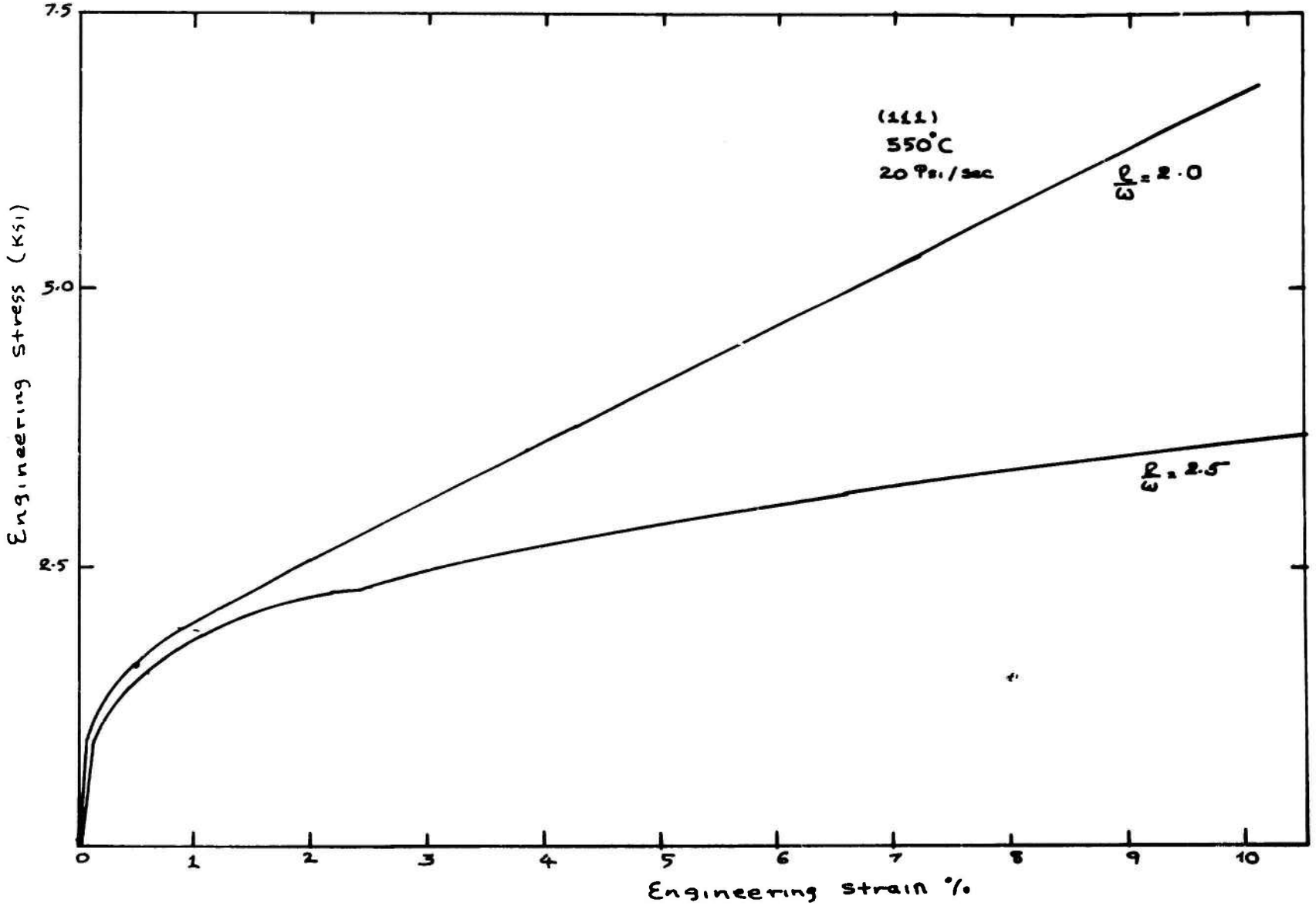

Fig. 5: Stress-strain curves for (111) orientation at ℓ/ω = 2.5 and ℓ/ω =2.0.

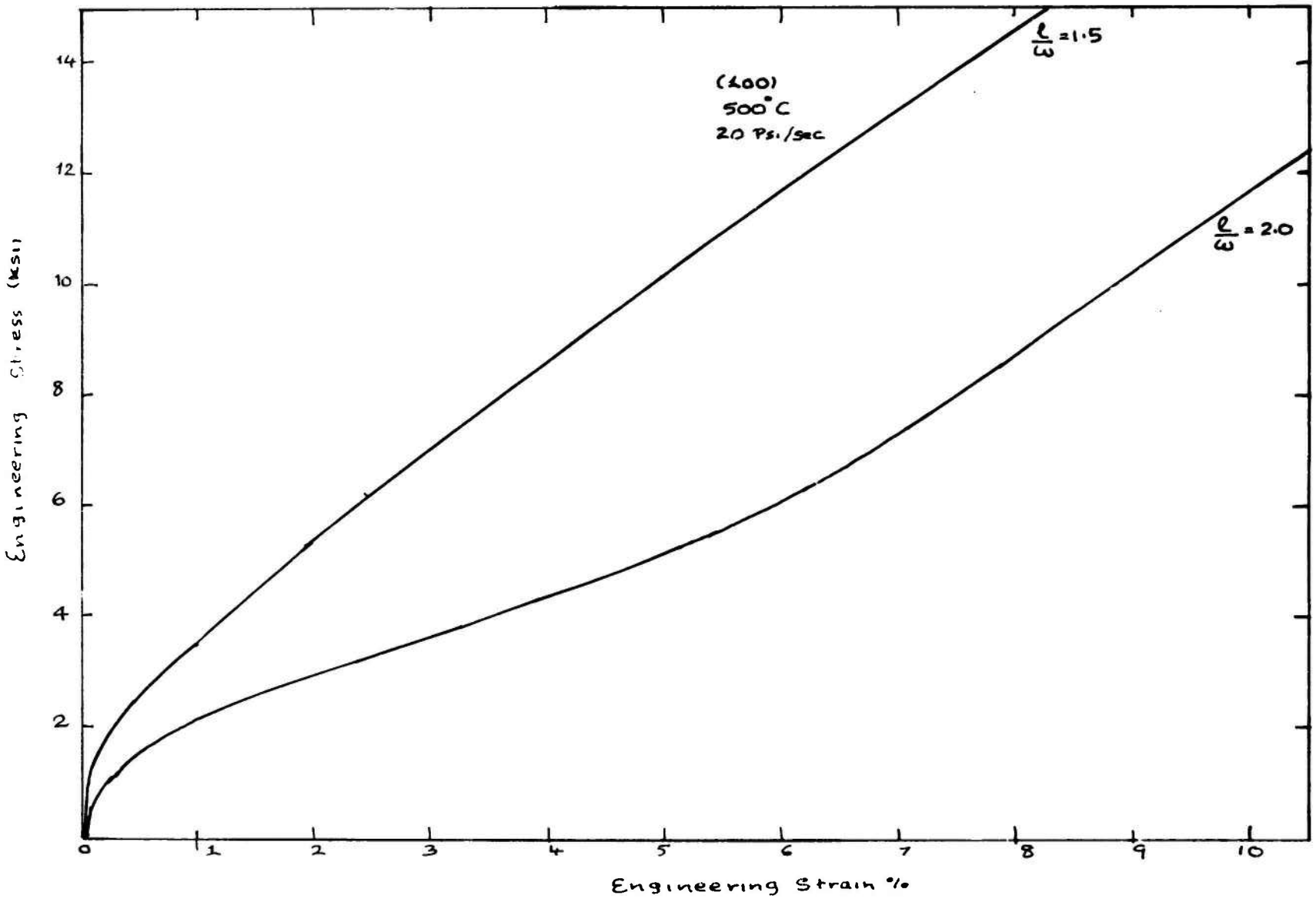

Fig. 4: Stress-strain curves for (100) orientation at ℓ/ω = 2.5 and ℓ/ω = 2.0.

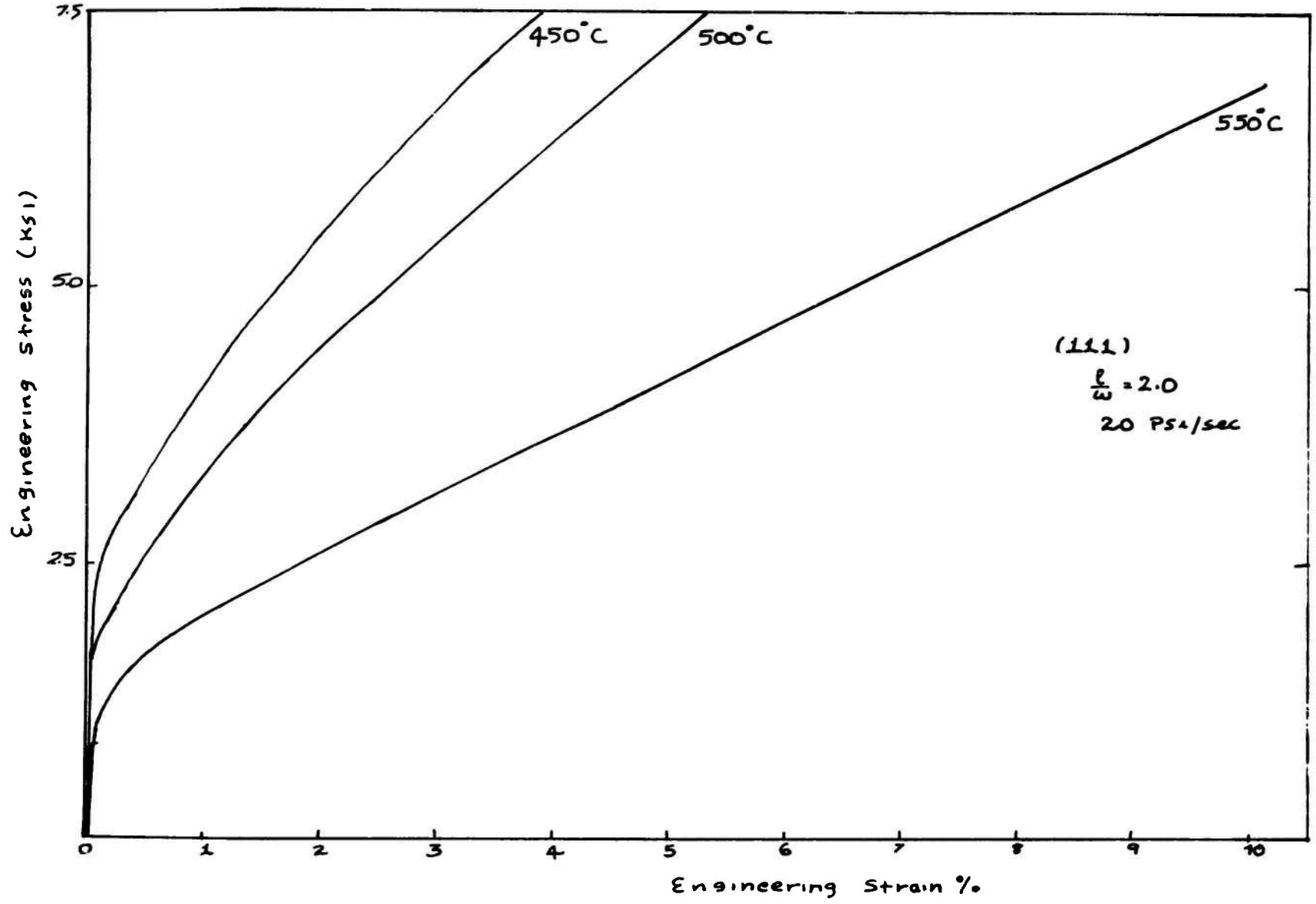

Fig. 3: Stress-strain curves for (111) orientation at 450°C, 500°C and 550°C.

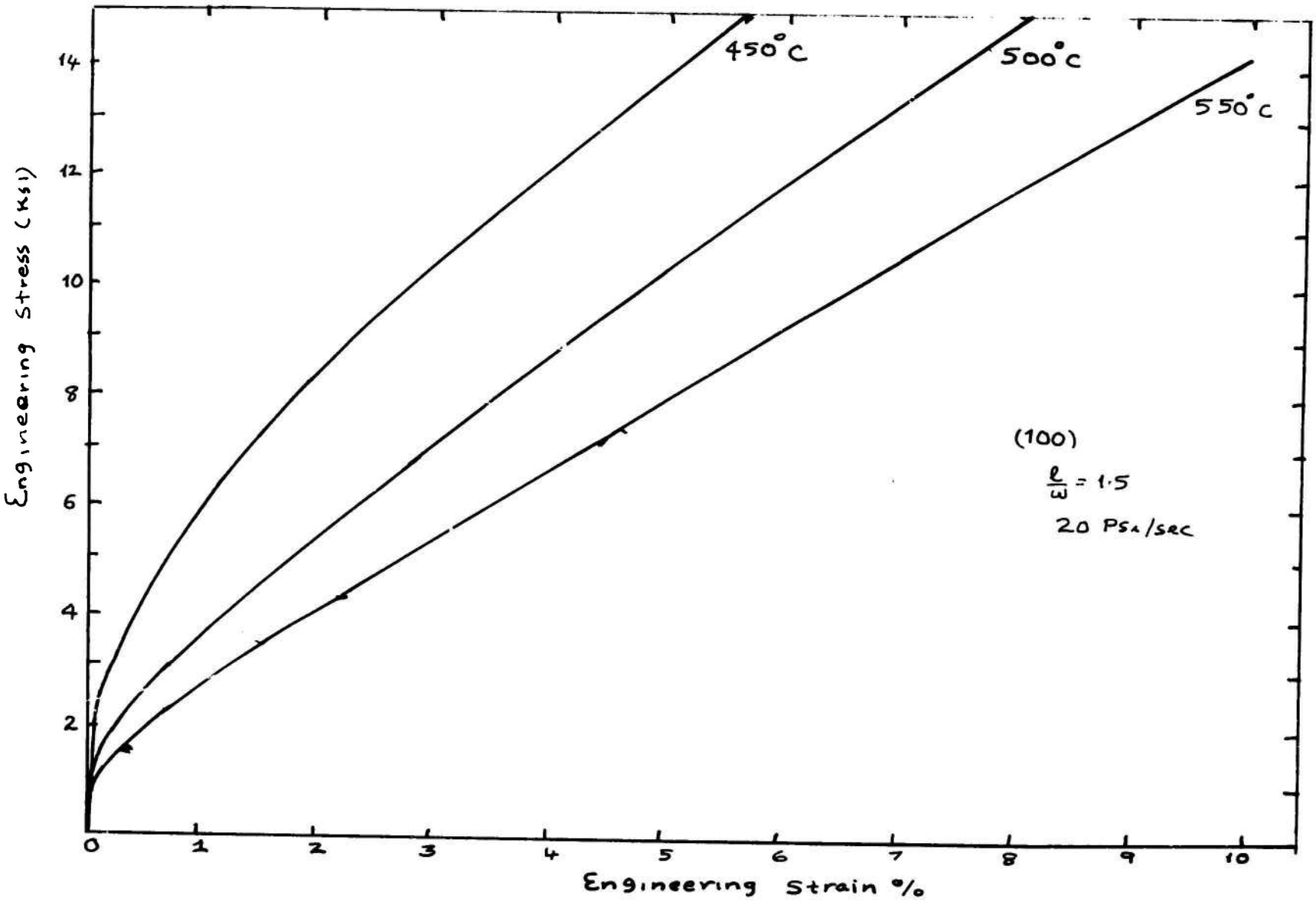

Fig. 2: Stress-strain curves for (100) orientation at 450°C, 500°C and 550°C.

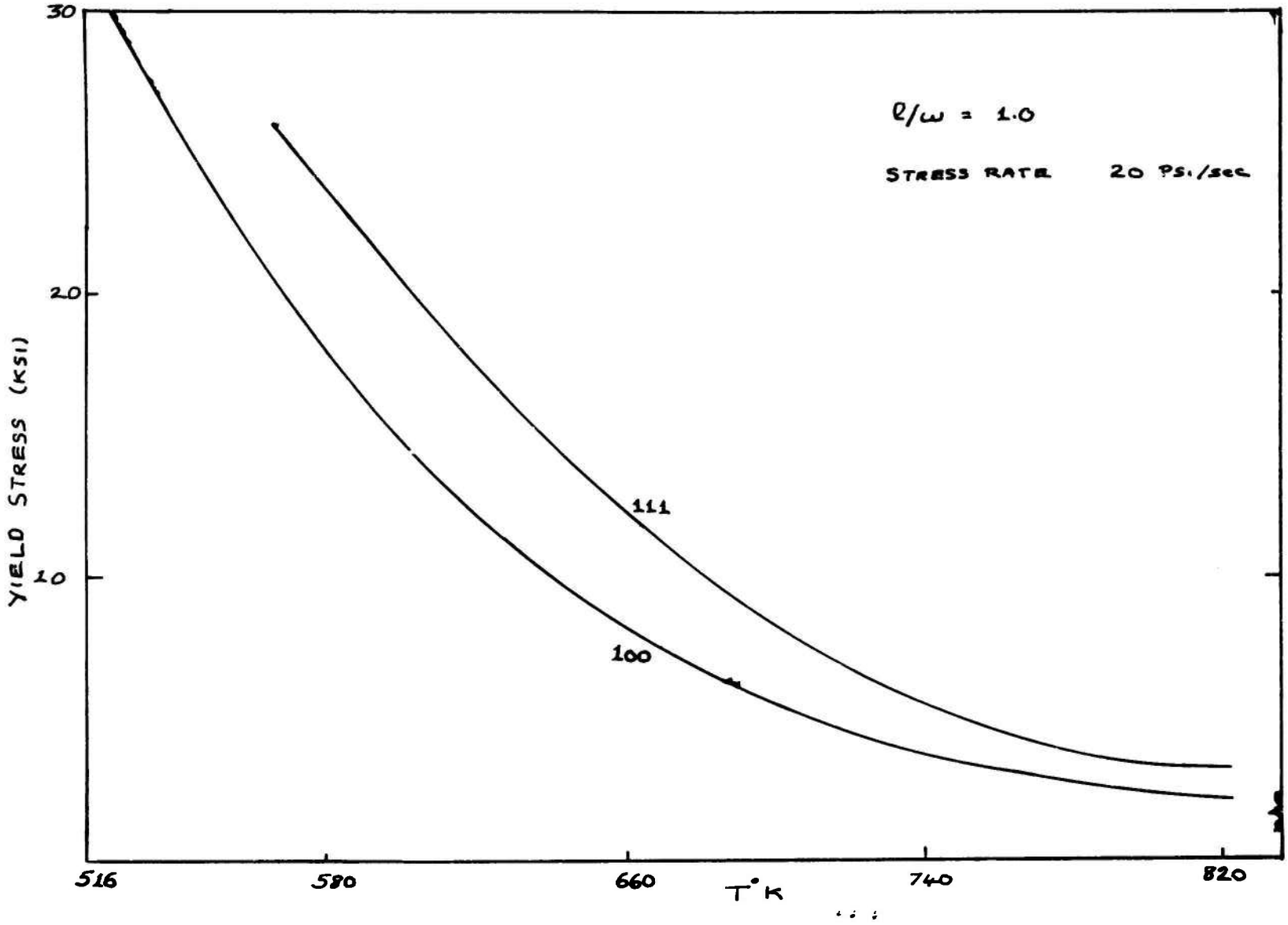

Fig. 1: Variation of yield stress with temperature over a temperature of 250°C to 550°C for (111) and (100) orientations.

d. 1 Surface and Interface IR Absorption

C. R. Crowell and S. Joshi

Effort during this quarter was directed toward production of a good sample and performing sufficient diagnostic measurements to ensure a meaningful measurement of dielectric constant of GaAs. During sample preparation the two deposition cycles used earlier were reduced to one by flipping the sample over during evaporation. This eliminated possible contamination of the sample surface between deposition cycles. Consequently, a sample with good electrical characteristics was obtained. The sample thickness was about 3 mils to simultaneously provide conveniently measurable thickness and capacitance.

To ensure that there was no bias dependent depletion layer thickness, the capacitance vs. bias curve shown in Fig. 1 was taken. The capacitance is independent of a bias up to 75 volts of either polarity at a frequency of 20 KHz. The electrical structure of the sample can be viewed as two metal-semiconductor barriers connected back to back. An applied bias of either polarity across the structure reverse biases one barrier and forward biases the other. The results show that the Debye screening length asssociated with the majority carriers is large compared to the sample thickness, since the applied bias does not affect the capacitance of the structure. However, when one of the barriers is forward biased, minority carriers are injected and hence the conductance of the sample is expected to increase with the applied bias. This indeed has been observed and the conductance vs. bias plot is also shown in Fig. 1. The spike in conductance near 75 volts occurs at an average field of 10^4 V/cm across the sample and may be related to the Gunn effect.

The capacitance vs. frequency curve is shown in Fig. 2. The capacitance increases by about 4% of its value at the high frequency as the frequency is changed from 1 MHz to 20 Hz. The conductance G vs. frequency plot is also shown in Fig. 2. These capacitance and conductance changes may be explained by the presence of deep impurity Cr levels which were introduced to compensate the GaAs to produce the high resistivity ($\sim 10^8$ ohm-cm) material under investigation.

The conductance rise is of the general form expected for a series resistance of approximately 100Ω, and the low frequency conductance is that expected from the bulk resistivity. One might expect a series resistance of this order of magnitude from deep level charging effects near the metal electrodes. At liquid nitrogen temperature, this series resistance effect is enhanced and the capacitance shows what we feel is an anomalous drop at high frequencies which is shown in Fig. 2 by a dotted line for a sample of slightly lower area.

The capacitance vs. temperature measurements were performed to verify earlier published data[1]. The measurements were performed at 50 KHz where C vs. ω is still flat. A linear relationship of capacitance vs. temperature was obtained. The rate of change of capacitance with temperature is 2.0×10^{-4} $\mu f / \mu f/^{o}K$ based upon the capacitance extrapolated to $0^{o}K$.

The dielectric constant determined from the above measurements was 12.4 ± 0.12 or with a possible error of 1%.

We plan to repeat the above measurements on another sample of the same material and using material from another source. We also plan to improve the precision of the area and thickness measurements.

References

(1) K. S. Champlin and G. H. Glover, Applied Physics Letters, vol. 12, pp. 231, 232 (1968).

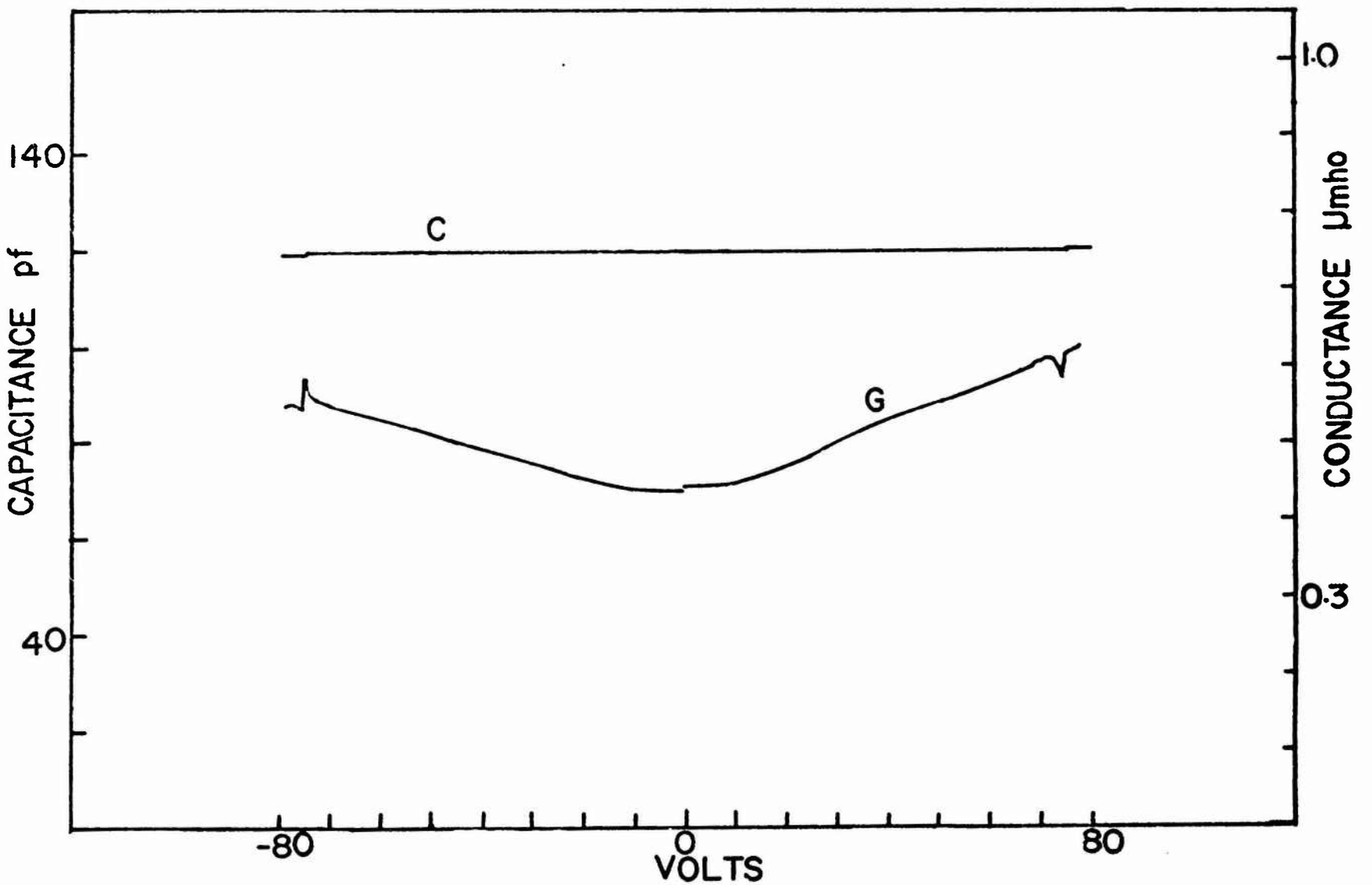

Fig. 1 Voltage dependence of capacitance C and conductance G at 30 KHz for a GaAs dielectric capacitor at room temperature.

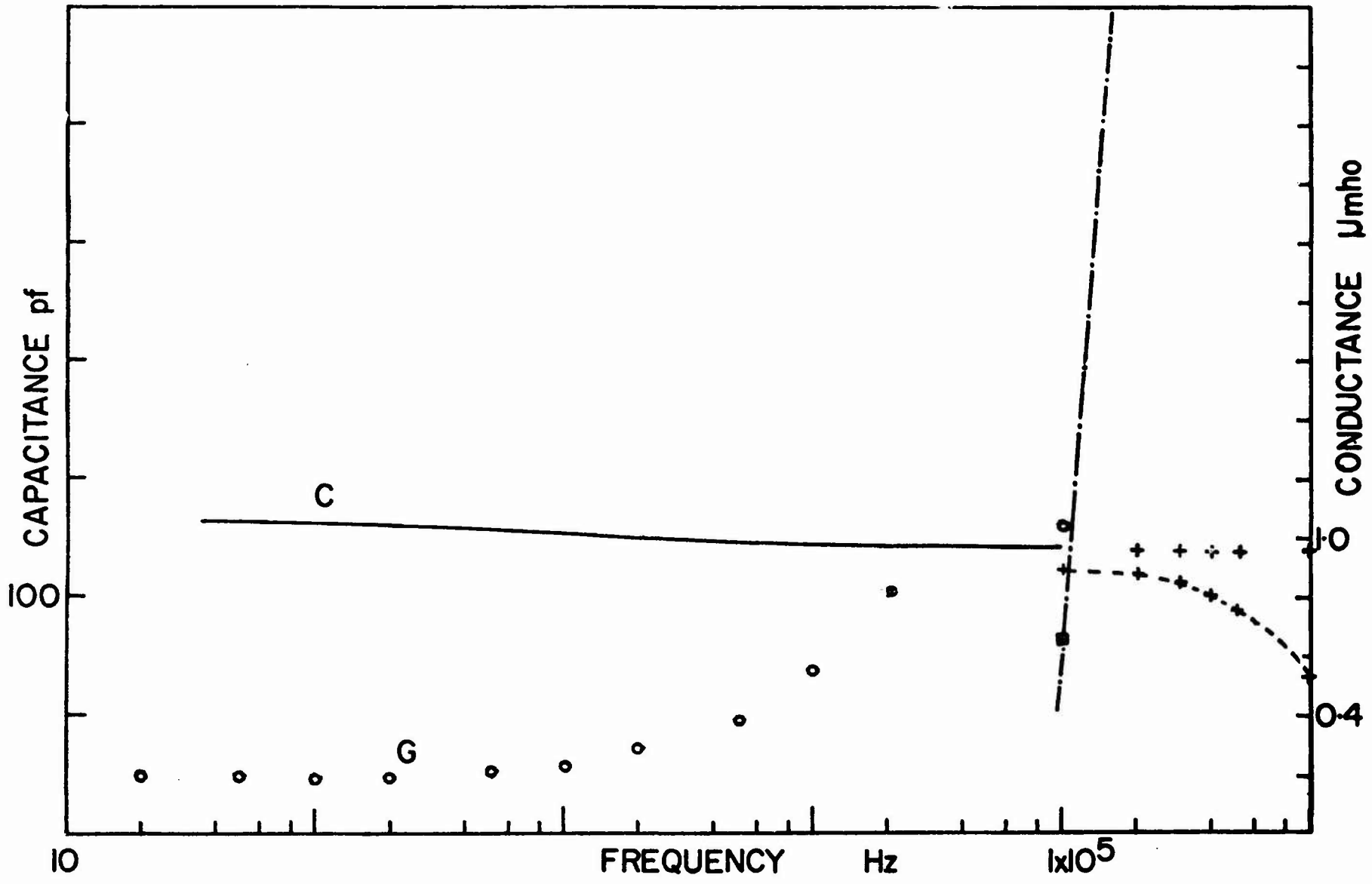

Fig. 2 Frequency dependence of capacitance C and conductance G. Legend: —— ++ C @300°K, - - - +++ C @77°K, ooo G @ 300°K, -·-·-· G @ 77°K.

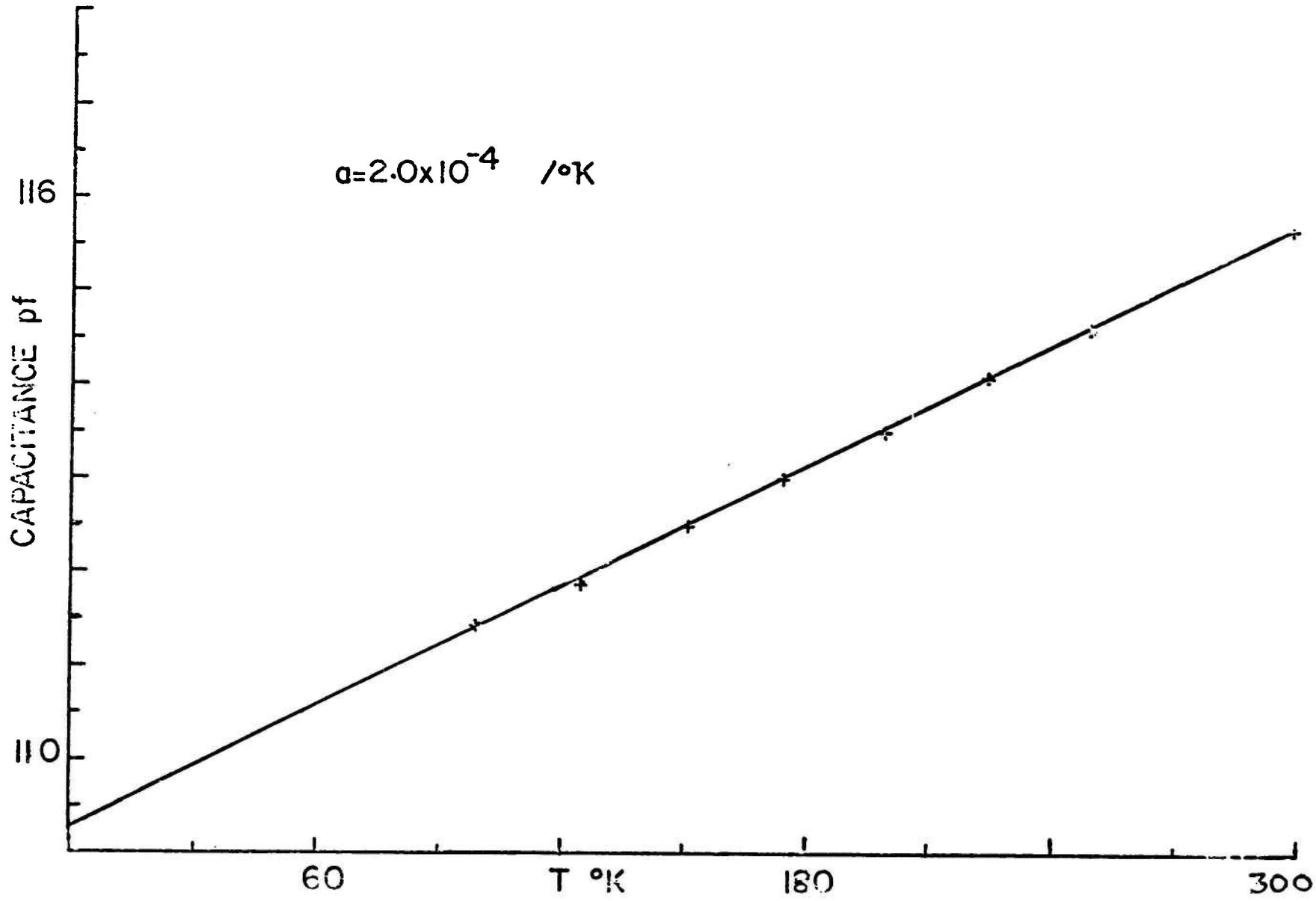

Fig. 3 Temperature dependence of dielectric capacitance at 50 KHz. Slope a = 2.0 x 10^{-4} /°K.

d. 2 Study of Defects in II-VI Compounds

F. A. Kroger, S. S. Chern and H. R. Vydyanath

The measurements of the self diffusion of Cd and Te in pure and indium doped CdTe have been completed.

We have succeeded to explain these data as well as results from high-temperature Hall effect measurements and from Hall effect measurements on cooled crystals due to de Nobel on the basis of a defect model with dominant defects $V_{Te}^{\cdot\cdot}$, $Cd_i^{\cdot\cdot}$ at high p_{Cd}, $V_{Cd}^{''}$, $V_{Cd}^{'}$, $Te_i^{'}$ at low p_{Cd}, and $(Cd_i V_{Cd})^x$ at all p_{Cd}.

Defect formation reactions and the corresponding mass action relations are given in Table I. Parameters of K(T) are given in Table 2.

Table I

Defect Formation Reactions for CdTe and the Corresponding Mass Action Relations

$CdTe + e' \rightarrow Cd(g) + Te_i^{'}$	$K_{TeI}^{'} = [Te_i^{'}]p_{Cd}/[e']$
$Cd_{Cd}^x + e' \rightarrow Cd(g) + V_{Cd}^{'}$	$K_{CdV}^{'} = [V_{Cd}^{'}]p_{Cd}/[e']$
$CdTe + 2e' \rightarrow Cd(g) + Te_i^{''}$	$K_{TeI}^{''} = [Te_i^{''}]p_{Cd}/[e']^2$
$Cd_{Cd}^x + 2e' \rightarrow Cd(g) + V_{Cd}^{''}$	$K_{CdV}^{''} = [V_{Cd}^{''}]p_{Cd}/[e']^2$
$Cd(g) \rightarrow Cd_{Cd}^x + V_{Te}^{''} + 2e'$	$K_{TeV}^{''} = [V_{Te}^{\cdot\cdot}][e']^2/p_{Cd}$
$Cd(g) + V_i^x \rightarrow Cd_i^{\cdot\cdot} + 2e'$	$K_{CdI}^{''} = [Cd_i^{\cdot\cdot}][e']^2/p_{Cd}$
$V_{Cd}^{''} \rightarrow V_{Cd}^{'} + e'$	$K_{a_2V} = [V_{Cd}^{'}][e']/[V_{Cd}^{''}]$
$O \rightarrow e' + h^{\cdot}$	$K_i = [e'][h^{\cdot}]$
$CdTe \rightarrow Cd(g) + \frac{1}{2}Te_2(g)$	$K_{CdTe} = p_{Cd}p_{Te_2}^{\frac{1}{2}}$

Table 2

Parameter values for equilibrium constants of the reactions given in Table 1

$$K = K_o \exp(-H/kT)$$

K	K_o (site fraction, atm)	H (eV)
$K_{TeI}^{'}$	3.94×10^3	1.19
$K_{CdV}^{'}$	9.8×10^7	2.08

K	K_o(site fraction, atm)	H(eV)
K''_{CdV}	9.18×10^{9}	1.42
K_{a_2V}	1.07×10^{-2}	0.66
K_i	3.1×10^{-2}	1.92
$K''_{CdI}+K''_{TeV}$	7.65×10^{-7}	1.86
K_{CdTe}	5.7×10^{9}	2.98

With these constants we can calculate defect isotherms for pure and indium doped crystals in equilibrium with an atmosphere of fixed p_{Cd} or p_{Te_2}. For level positions as given in Fig. 1 of Quarterly Report No. 1, and assuming that atomic defects can be frozen in but that electronic reactions reach equilibrium at all temperatures, we can also construct isotherms for cooled (quenched) crystals. Figure 1 shows the regions of high resistivity predicted for undoped CdTe and for CdTe doped with 2.7×10^{17} and 3.6×10^{18} donors(indium) cm^{-3}. The figure also indicates the locus of points($\sigma = 0$) with composition CdTe and $CdTe\text{-}In_2Te_3$.

As indicated by Gentile et al[1] at these points precipitation must be expected to be minimal. If precipitation occurs, the fields of high resistivity become narrower. The least precipitation is expected at the lowest equilibration temperature. Parameters describing diffusion constants of individual defects as functions of T are given in Table 3. For comparison, the parameters for $D_{V''_{Cd}}$ in CdS are also given

Table 3

Parameters of defect diffusion constant $D_j = D_j^o \exp(-H/kT)$

	$D^o cm^2/sec$	H(eV)
$D_{V'_{Cd}}$	1.01/f	1.13
$D_{V''_{Cd}}$	66.7/f	1.54
$D^*_{Cd_i^{\cdot\cdot}}/[D_n^{\cdot\cdot}]_{total} = D_{Cd_i^{\cdot\cdot}} \frac{[Cd_i^{\cdot\cdot}]}{[D_n^{\cdot\cdot}]_{total}}$	2.63×10^{2}	1.49
$(D_{V''_{Cd}})_{CdS}$	4.39	1.48

f = correlation coefficient ≈ 1.

For undoped CdTe, chemical diffusion establishing Cd-excess can be described by a diffusion coefficient D_{chem} which is related to the Cd tracer self diffusion coefficient, D^{*}_{Cd}, by

$$D_{chem} = kD_{Cd_i^{\cdot\cdot}} \cdot [Cd_i^{\cdot\cdot}]/[V_{Te}^{\cdot\cdot}] = 3D^{*}_{Cd}/[V_{Te}^{\cdot\cdot}]$$

where k is a numerical constant (≈ 3) accounting for the neglect of conduction terms in describing the diffusion process which involves ambipolar diffusion and therefore requires terms dependent on the electric field. For donor-doped CdTe the corresponding relation is

$$D_{chem} = \frac{1}{C_e}\left(C_{V'_{Cd}} D_{V'_{Cd}} + 4C_{V''_{Cd}} D_{V^{\cdot\cdot}_{Cd}}\right) + \left(D_{V'_{Cd}} F' + D_{V''_{Cd}} F''\right)$$

where F' and F'' are functions of

$$dC_{Te'}/dC_{V'_{Cd}} \quad \text{and} \quad dC_{V''_{Cd}} / dC_{V'_{Cd}} \; .$$

These formulae describe the chemical diffusion process correctly both as far as the absolute value and the temperature dependence is concerned.

e.1 Theoretical Studies of Absorption Mechanisms in IR Window Materials

R. W. Hellwarth and M. Mangir

e.1.a Linear and Nonlinear Electric Moments

This quarter we continued the search for definitive experimental methods for determining whether or not, in a given window material, multi-phonon absorption is mediated mainly or in part by a nonlinear relation between the macroscopic electric moment per unit volume (i.e., polarization density) and the local ionic displacements. We have analyzed many effects for this purpose, such as the shifts of ω_{TO} and ω_{LO} with temperature and pressure, microwave harmonic and sub-harmonic generation, microwave scattering and dielectric constant variations. Perhaps the mose promising method, which we are pursuing presently, is the measurement at two different temperatures of the complete spectrum of the imaginary part of the electric susceptibility. We are developing a test for the nonlinear moment from this data by analyzing the sum rules we derived in the Appendix for e.1 of the previous quarterly report (and to be published in the Proceedings of the 1973 Symposium on Damage in Laser Materials, Boulder, Colorado, May 15, 16 (1973)).

e.1.b Lyddane-Sachs-Teller (LST) Relations

We have performed a survey of the literature on KCl, KBr, NaCl, LiF, GaAs, GaP, and InP to see whether existing data on these materials is consistent with the LST relation

$$\omega_{LO}^2/\omega_{TO}^2 = \epsilon_o/\epsilon_\infty$$

based on the linear-dipole-moment and harmonic-crystal approximations. We have found such great inconsistency in the data on ω_{TO}, ω_{LO} and ϵ_o that it is not possible to say whether any of these materials, except GaAs, satisfies the relation to within experimental error (typically $\sim 5\%$). The most reliable-appearing data on GaAs suggests that the relation is obeyed at room temperature but not at lower temperatures. We are investigating this further with Dr. Crowell who is remeasuring the most fallible number, ϵ_o, in the LST relation for GaAs.

f. 1 Temperature Dependent Absorption Measurements of GaAs

W. H. Steier, P. Christensen, S.T.K. Nieh, R. Joiner

Measurements of optical absorption in GaAs as a function of temperature have been performed over a temperature range extending from 30°C to 400°C. In these experiments GaAs samples were placed in a windowless oven designed for short-term temperature stability, and sample absorption was measured using calorimetric techniques. Experimental results were obtained at wavelengths of 9.28μ and 9.68μ using a CO_2 laser as the optical source. Bell Laboratories sample 55-1A and USC sample WA-1000 were used in the study; additional information on these materials can be found in the preceding quarter report. Both samples initially exhibited low optical loss ($\beta < 0.009$ cm^{-1}) and high resistivity ($\sim 10^8$ Ω-cm).

Typical absorption vs. temperature curves are shown in Fig. 1. The two samples were found to exhibit a very similar temperature dependence over the entire temperature range, and it is evident from the experimental results that two different absorption mechanisms influence the shape of the curves. Below 280°C the absorption coefficient shows only weak temperature dependence; however, at higher temperatures the loss varies approximately as $\exp(-\Delta E/kT)$ where $\Delta E \cong 0.57$ ev.

The high-temperature absorption is apparently due to thermally-generated free carriers. Support of this hypothesis is lent by the dashed curve in Fig. 1, which gives the calculated free carrier absorption for a semiconductor having a room-temperature resistivity of 10^8 Ω-cm and a fixed Fermi level lying 0.57 ev below the conduction band. The absorption mechanism at temperatures below 280°C has not as yet been determined.

Irreversable increases in absorption due to heating have also been observed. Figure 2 shows the large increase in room-temperature absorption obtained by heating a sample to 390°K in air for about two hours. The decrease in absorption produced by subsequent repolishing indicates that both surface and bulk changes take place during the heating process.

In addition, we note that the large peak at 9.8μ (due primarily to surface effects in Spectrum B coincides with smaller peaks in Spectra A and C. This suggests either that a measurable part of the loss in these samples is due to surface absorption, or that bulk and surface absorption mechanisms are closely related. Further investigation of surface loss is thus desirable.

We speculate that the observed surface loss is due to the formation during heating of a high-loss film on the GaAs surface. Experiments have now begun in which ellipsometric techniques, chemical treating, and controlled polishing and etching will be used in conjunction with calorimetric loss measurements in an effort to determine the thickness and composition of such films.

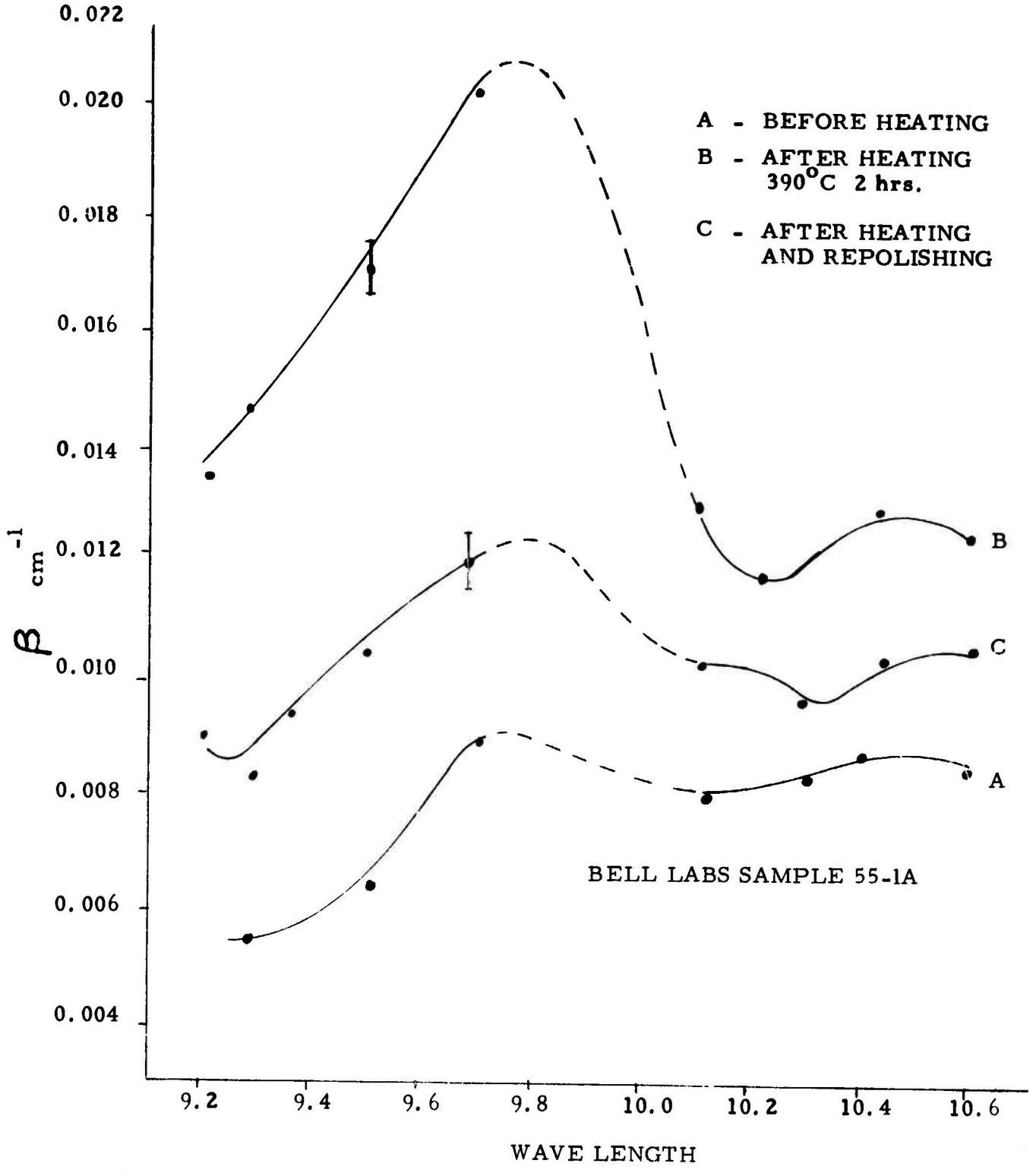

Fig. 2 Absorption spectrum of GaAs as a function of heat treatment and polishing.

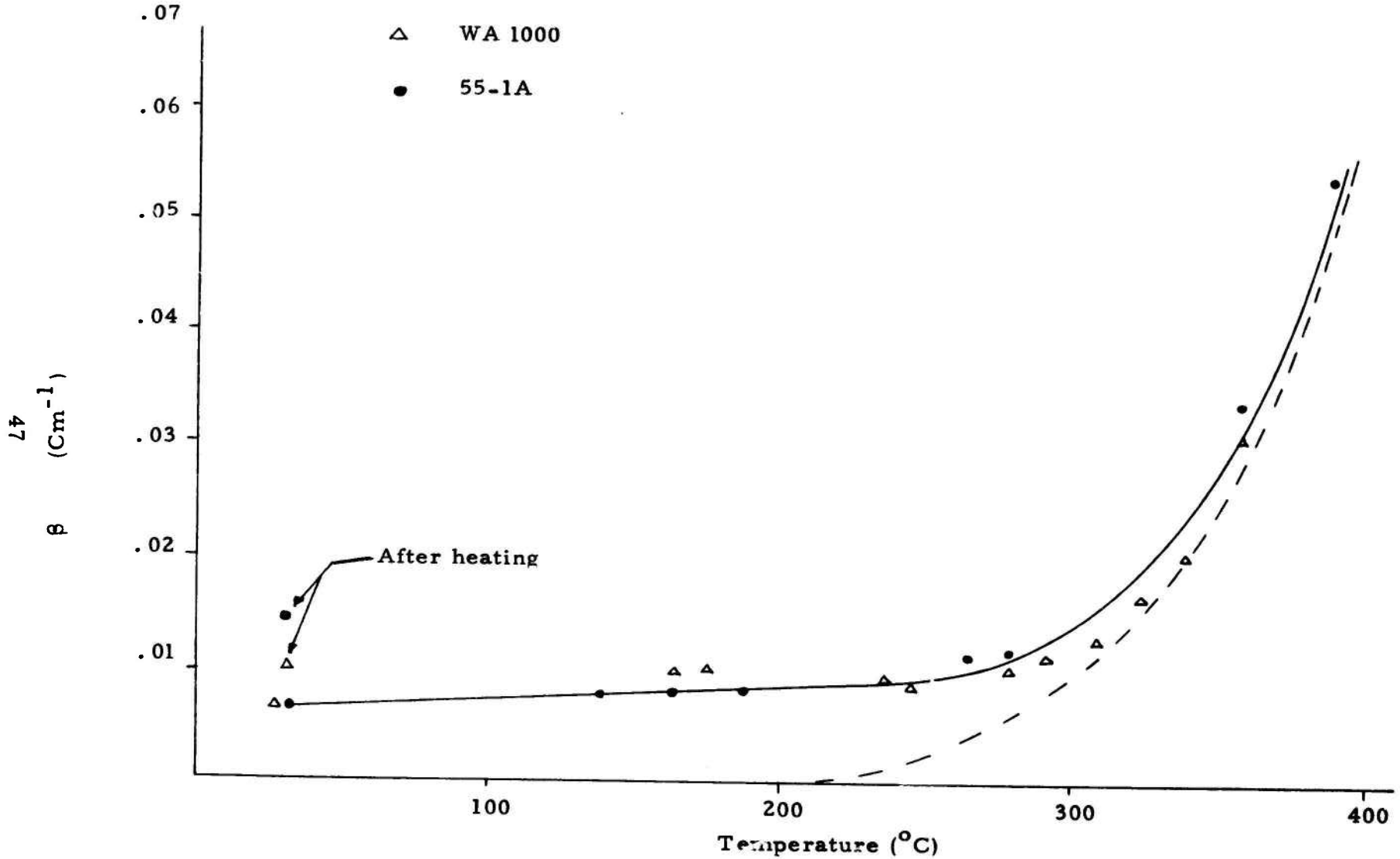

Fig. 1 Absorption constant at 9.28 μ of two GaAs samples as a function of temperature.

f.2 Alkali Halide Surface Studies with Acoustic Probe Techniques

J. H. Parks, D. Rockwell, T. Colbert

During this quarter, the investigation of techniques to couple acoustic surface waves to non-piezoelectric surfaces via a fluid layer has continued. The limitations of this process have to be clearly identified to assess its applicability to absorption measurements on KCl samples. A theoretical study has been underway and fluid coupling experiments are now beginning.

Controlled experiments of acoustic thermal detection have been nearly completed. Data presented in this report indicates the detection of resistive surface heat pulses of energy 12μJ and pulsewidths as short as 0.5 μsec. Experimental results are also included which suggest a new technique to observe the temporal development of thermal expansion which follows the surface absorption of a Gaussian shaped light pulse. These new results of acoustic thermal detection will be shown to provide useful analytic techniques to extend measurements of window material parameters.

a Fluid Coupling Surface Acoustic Waves

An experimental and theoretical study has been initiated to understand the limitations imposed by the fluid coupling process which will be used to couple acoustic surface waves to non-piezoelectric KCl surfaces. Relatively little analysis of this coupling process[1] is available in the literature which is applicable to the present research problem. Our analysis extends previous results to materials involved in this research including waves coupled from crystal quartz or Bismuth-Germanium-Oxide (BGO) substrates to KCl samples. Our primary concern is the stability of the coupling process to prevent phase noise and phase drift from obscuring the phase shift signals induced by the KCl absorption.

The fluid coupling process is shown in schematic form in Fig. 1a which indicates the acoustic wave excited and detected on a piezoelectric material by interdigital transducers and the coupling to and from the KCl surface via the fluid layer interface. Wave propagation within the fluid layer is a composite of surface waves in the solids and a longitudinal wave in the fluid: a layer wave. This acoustic wave propagation

is dispersive and the phase and group velocities of the layer wave depend strongly on the layer thickness, h. A variation of h introduces a phase change both by increasing or decreasing the distance traveled by the wave and also by a dispersive change in the wave velocity.

Layer Wave Calculations

Consider an acoustic wave propagating in a fluid layer bounded by two semi-infinite elastic solids. The additional boundary conditions introduce dispersion relations which relate the layer wave velocity in the fluid, v, and the thickness of the layer, h. These are given by[1]

$$(G-\cot\theta)(G+\tan\theta) = (G-F)(G-\cot 2\theta) \qquad (1)$$

where

$$F = \frac{\rho}{\rho_f}\left(\frac{v_t}{v}\right)^4\sqrt{\left(\frac{v}{v_f}\right)^2-1}\left\{\frac{\left[2-\left(\frac{v}{v_t}\right)^2\right]^2}{\sqrt{1-\left(\frac{v}{v_\ell}\right)^2}} - 4\sqrt{1-\left(\frac{v}{v_t}\right)^2}\right\}$$

and

$$G = \frac{\rho'}{\rho_f}\left(\frac{v'_t}{v}\right)^4\sqrt{\left(\frac{v}{v_f}\right)^2-1}\left\{\frac{\left[2-\left(\frac{v}{v'_t}\right)^2\right]^2}{\sqrt{1-\left(\frac{v}{v'_\ell}\right)^2}} - 4\sqrt{1-\left(\frac{v}{v'_t}\right)^2}\right\}$$

ρ and ρ' being the densities of the two solids, ρ_f the fluid density, v_ℓ and v'_ℓ (v_t and v'_t) the longitudinal (transverse) velocities in the solids, and v_f the sound velocity in the fluid. The two solids are assumed to be isotropic and the fluid has zero shear modulus. The dependence on the layer thickness, h, is included in the function θ given by

$$2\theta = \frac{2\pi}{\lambda}\, h\sqrt{\left(\frac{v}{v_f}\right)^2-1}$$

where λ is the acoustive wavelength.

A computer study of these dispersion relations was performed for the following three different situations. The data used in Eq. (1) is listed in Table 1.

1. Layer Wave Propagation in a quartz-fluid-quartz structure. In this case

$G \equiv F$ and Eq. (1) describes two families of dispersion curves which follow from the independent equations

$$G = \cot \theta \qquad \text{and} \qquad G = -\tan \theta \,. \tag{2}$$

Group and phase velocity curves are shown in Figs. 2a and 2b for each dispersion relation. The group velocity was calculated from the phase velocity using the relationship $v_G \simeq v + k(dv/dk)$.

2. Layer wave propagation in a quartz-fluid-KCl structure. The group and phase velocity curves are shown in Figs. 3a and 3b. This was chosen as an example of a layered structure having a large mismatch in surface wave velocities as shown in Table 1.

3. Layer wave propagation in a BGO-fluid-KCl structure. Group and phase velocities are shown in Figs. 4a and 4b. This was chosen as an example for which the surface wave velocities were well matched.

These initial calculations indicate several important characteristics of the slope of the velocity dispersion curves (dv/dh) and the density of acoustic wave modes. It is clear for example that the damping of high frequency mechanical vibrations may be necessary to avoid dispersive changes in phase velocity associated with changes in layer thickness. These phase velocity changes could mask temperature induced phase change signals. In Fig. 3a the indicated slope yields

$$\frac{\delta v}{v} \simeq -(.3)\frac{\delta h}{\lambda}$$

which shows that the percentage change in phase velocity for $\delta h \simeq 1\mu$ and $\lambda = 25\mu$ may be comparable to thermally induced phase changes in KCl. However the effects of mechanical vibrations will be significant only for vibrations which have a period comparable to the measurement time. In our case this will generally be high frequency microphonics (>50 KHz) and the amplitude of these vibrations can be considerably reduced by structural design and isolation.

Acoustic pulse measurements suggest two possibilities which follow directly from the group velocity dispersion curves. In Fig. 3b the points A and B represent possible operating points for layer wave propagation. Point A offers the advantage of working in a dispersive region for which the slope (dv/dh) varies very slowly about a zero value. At point B the dispersion curve has a positive slope, and the phase variation

$$\frac{\delta \varphi}{\varphi} \simeq \frac{\delta h}{h} - \frac{\delta v}{v}$$

will be reduced by the compensating effects of a change in layer thickness and the corresponding dispersive change in velocity. These characteristics do not occur for the phase velocity and thus CW measurements. Pulsed measurements, although generally less sensitive, may be useful at high repetition rates and pulsewidths (~1 ms) for which a transfer oscillator can accurately detect the FM pulse modulation induced by the temperature changes in the KCl.

Layer Wave Experiments

During this quarter, instrumentation has been completed for a series of experiments to determine the feasibility of using a fluid coupling process. We have received assistance in this effort from Dr. Hal Bennett, Dr. David White and Mr. Raymond King of the Michaelson Laboratory, NWC, China Lake. The series of experiments will begin with a study of the inherent stability of the coupling process. This will be investigated using the quartz-fluid-quartz configuration shown in Fig. 1b. The ends of the quartz substrates in contact with the fluid are coated with a metallic film to prevent coupling via the piezoelectric fields. The lower quartz piece will be mounted as shown in Fig. 1c, with a micrometer translation to vary the dimensions of the fluid layer region. The coupling experiments which include quartz-fluid-KCl and BGO-fluid-KCl will follow these initial studies.

The measurements to be considered in these experiments are

1. phase noise introduced by mechanical vibrations or evaporation
2. coupling efficiency dependence on type of fluid, length of coupling layer, and surface wave velocity mismatch
3. the effects of multimode operation, mode jumping, and the possibility of inducing single mode operation.

These measurements will be taken by detecting the relative phase shift as a function of layer thickness. Data analysis will relate the measured phase to the characteristics of the dispersion curves.

b Acoustic Temperature Detection

A paper is in preparation which includes recent results of our detector studies using a single mode CO_2 laser source and a quartz substrate detector. Several experimental results which have not been discussed previously are presented here. These will be shown to have important applications to our studies of IR window materials.

Detection of Surface Heat Pulses

Resistive heating was chosen for short pulse measurements as a calibrated source of energy deposition with variable pulse width. An aluminum resistive film was positioned between two interdigital transducers as shown in Fig. 5 and square voltage pulses were applied of varying amplitude and pulsewidth. Fig. 6a shows recorded data of phase changes which have been induced by resistive heating pulses of 50-900μsec. The phase change is measured with a double balanced mixer which provides a voltage output, $V \simeq 0.2 \sin(\Delta\varphi)$, related to the induced phase variation $\Delta\varphi$. These phase changes range from 20 to 80 millirad. Also shown in the same figure is a current pulse of ~1.1 amp for the 900μsec pulse.

Fig. 6b shows a phase change of 30 millirad induced by a 1.1 amp pulse of 120 μsec. The initial portion of the phase change (< 20μsec) exhibits a curviture which will be of particular importance when these techniques are applied to the measurement of thin film properties. This timescale of ~20μsec is just the time necessary for heat deposited at the surface to diffuse downward a distance of ~10μ and fill the volume probed by the acoustic wave. Since the heated volume probed is increasing, the rate of change of temperature, which is proportional to the input power per unit volume, is initially large and eventually levels off at a rate determined by the power dissipated in the acoustic wave volume. This effect of heat diffusion is observable only because the power is initially deposited on the surface and the acoustic wave technique is extremely sensitive to the volume which is probed.

Thin film absorption is another example of a surface heat source. If absorption is a dominant energy loss mechanism for radiation passing

through the film, similar phase change behavior can be expected. However, if photoconductivity is a more important loss, the phase variation will exhibit completely different characteristics. The loss mechanism is in question for Ge films on KCl substrates and collaborative studies of this problem are being planned with Dr. Hal Bennett, NWC, China Lake.

Figs. 7 and 8 are data of the shortest surface heat pulses obtained on Y-cut quartz detecting substrates. For these pulsewidths the transit time of the phase change signal from the resistor to transducer is $\sim 3\mu$ sec as shown in Fig. 7, which also includes the current pulse. In Fig. 8 the variation of energy deposition is indicated by the signal pulse heights which scale directly proportional to the energy for these short pulses.

Dynamics of Thermal Expansion

It was indicated in an earlier report[5] that the phase change signal is proportional to the sum of temperature coefficients $\Delta\varphi \sim (\frac{1}{\ell}\frac{d\ell}{dT} - \frac{1}{v}\frac{dv}{dT}) = (\alpha_L - \alpha_V)$. This is rigouously true only for a substrate which undergoes a uniform temperature change. When a laser beam with a Gaussian radial profile is absorbed at the quartz surface, a nonuniform temperature distribution results. In this case, the cooler surface regions outside the beam spotsize constrain linear thermal expansion and the surface distorts transversely from induced stresses. This affects the induced phase change signal by reducing the effect of the thermal expansion coefficient, α_L, until heat diffusion extends the heat throughout an area larger than the spotsize. Thus, the thermal expansion evolves in time and this time dependence is included in the phase change signal.

An example of this is indicated by the data shown in Fig. 9. These data represent phase change signals induced by a TEM_{oo} 10.6μ laser source of spotsize $\simeq$ 3mm. The radiative pulsewidth range is indicated and was controlled by a camera shutter. These results for Y-cut and ST-cut crystal quartz emphasize the effects of the evolution of thermal expansion. The orientation of ST-cut quartz is so chosen that the coefficients $\alpha_L = \alpha_V$. For uniform temperature changes in an ST sample the phase is stable, $\Delta\varphi = 0$, since the expansion and velocity

effects cancel each other. However, in our case, the cancellation is prevented since the expansion is initially absent, and the induced phase change results as in Fig. 9. Identical irradiation conditions are shown in Fig. 9 for Y-cut quartz which exhibits a larger phase change and quite different characteristics for times when diffusion is important. In particular the ratio of the initial $\Delta\varphi$ slope for Y-cut and ST-cut shown in Fig. 9 is found to be the same as the ratio of the velocity temperature coefficients, α_V, which supports these conclusions.

The direct measurement of the dynamics of thermal expansion is an important consideration for window material properties. The effects of clamped expansion have been shown to produce optical phase distortion in transmitted beams. This acoustic wave technique may offer the possibility of direct measurement of the material stresses which produce these optical distortions. Experiments for several different crystal orientations in quartz are planned. These effects will be measured by varying the radiative spotsize and pulsewidth to change the effects of thermal expansion. The data reduction will parameter fit the phase change $\Delta\varphi$ to an assumed growth function for α_L. If this technique works reliably for the quartz data, this will provide some confidence that it can be applied to window material studies.

REFERENCES

1. P. W. Staecher and W. C. Wang, J. Acoust. Soc. Am. 53, 65 (1971) (includes references to additional articles describing fluid coupling).

2. O. L. Anderson, In Physical Acoustics (W. P. Mason, ed.) Vol. IIIB, pp. 43-97. Academic Press, New York, 1965.

3. Landolt-Bjorstein, (Springer-Verlag) New Series-Group III, Vol. 1, Berlin, Heidelberg, New York, 1966, Vol. 2, 1969.
4. E. G. Spencer et al. Appl. Phys. Letters 9, 290 (1966).
5. F. A. Kroger, J. H. Marburger et al. Electronic Sciences Laboratory, University of Southern California, "IR Window Studies", Quarterly Technical Report No. 3 (December-February 1973) AFCRL TR-73-0325, Contract No. F19628-72-C-0275, ARPA Order No. 2055 (29 September 1972).

TABLE 1

DATA FOR LAYER WAVE PROPAGATION

AT FREQUENCY 120 MHz

	Quartz[(a)]	BGO[(b)]	KCl[(c)]
Surface Wave Velocity $v_s \times 10^{-5}$(cm/sec)	3.159	1.708	1.74
Longitudinal Velocity $v_\ell \times 10^{-5}$(cm/sec)	6.05	3.42	3.88
Shear Velocity $v_t \times 10^{-5}$(cm/sec)	4.01	1.77	2.17
Density ρ (g/cm^3)	2.65	9.23	1.988
Fluid Velocity	$v_f = 1.5 \times 10^5$ cm/sec		

(a) Quartz

v_ℓ, v_t taken from Ref. 2, v_s calculated from data given in Ref. 3 for Y-cut, propagation in X direction

(b) BGO (Bismuth Germanium Oxide)

v_ℓ, v_t taken from Ref. 4 for propagation [110] direction, v_s calculated from data given in Ref. 3 for [110] propagation.

(c) KCl

v_ℓ, v_t taken from Ref. 2, v_s calculated from data given in Ref. 3 for propagation in [001] plane, [100] direction.

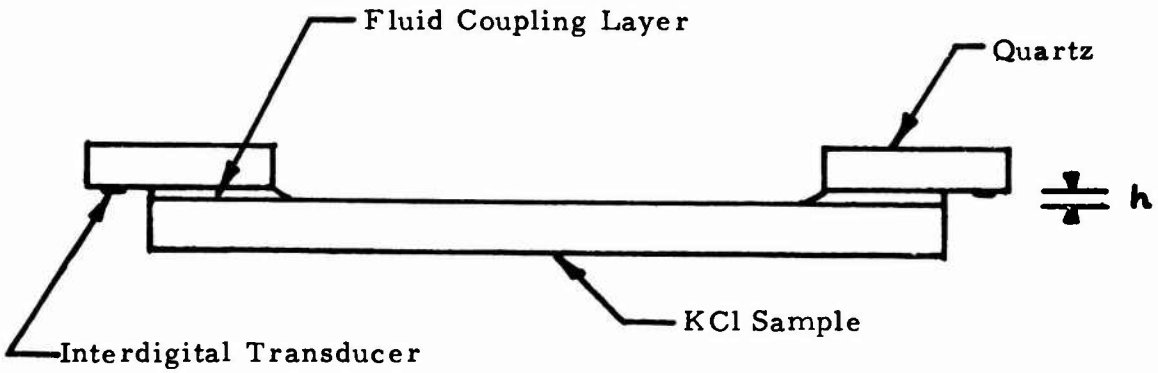

Figure 1a. Fluid coupling layer configuration

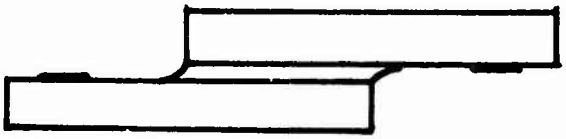

Figure 1b. Quartz-Fluid-Quartz coupling configuration

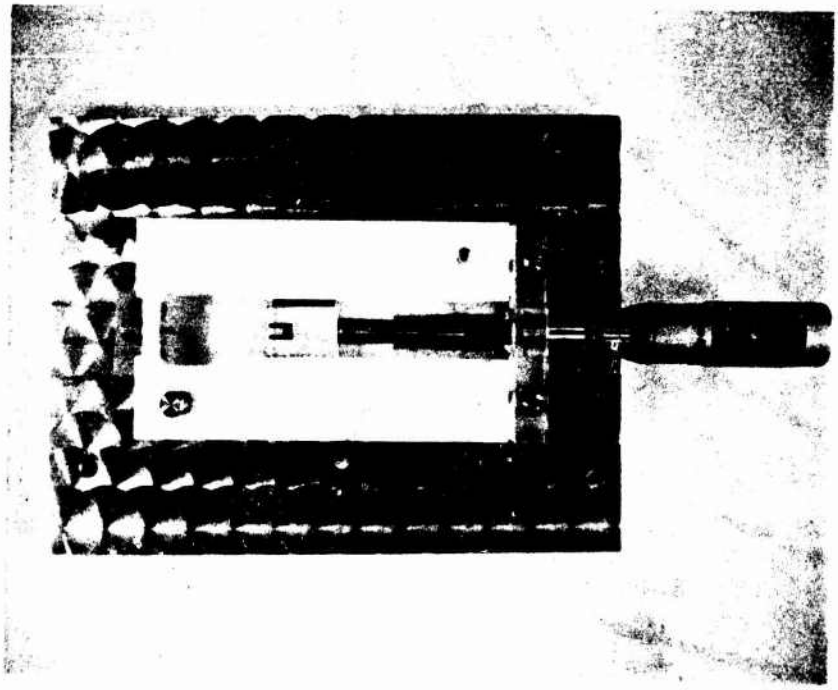

Figure 1c. Fluid coupling experimental assembly showing lower quartz transducer and translation micrometer

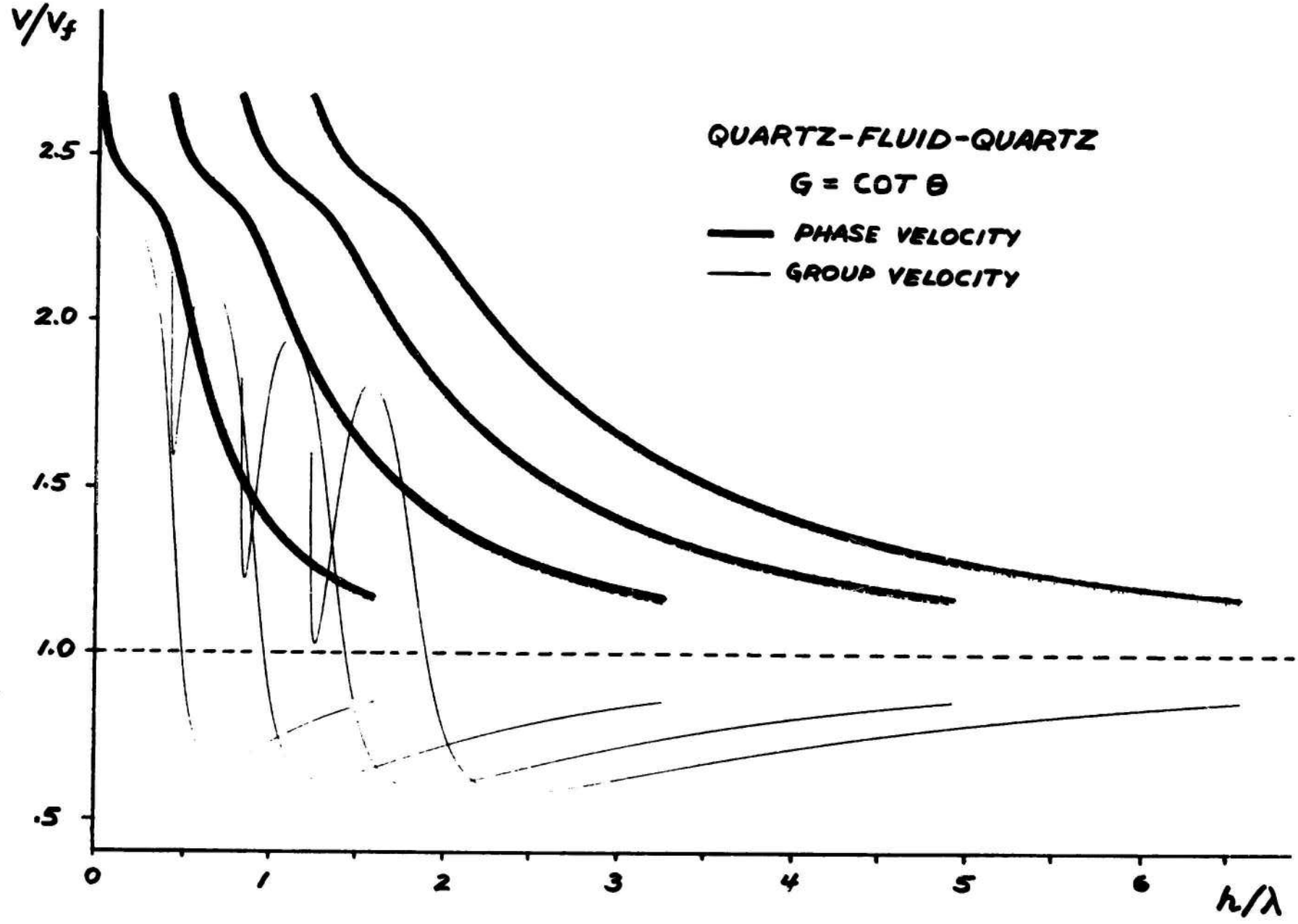
V/Vf
2.5
2.0
1.5
1.0
.5
0
1
2
3
4
5
6
h/λ
QUARTZ-FLUID-QUARTZ
G = COT θ
PHASE VELOCITY
GROUP VELOCITY

FIGURE 2a.

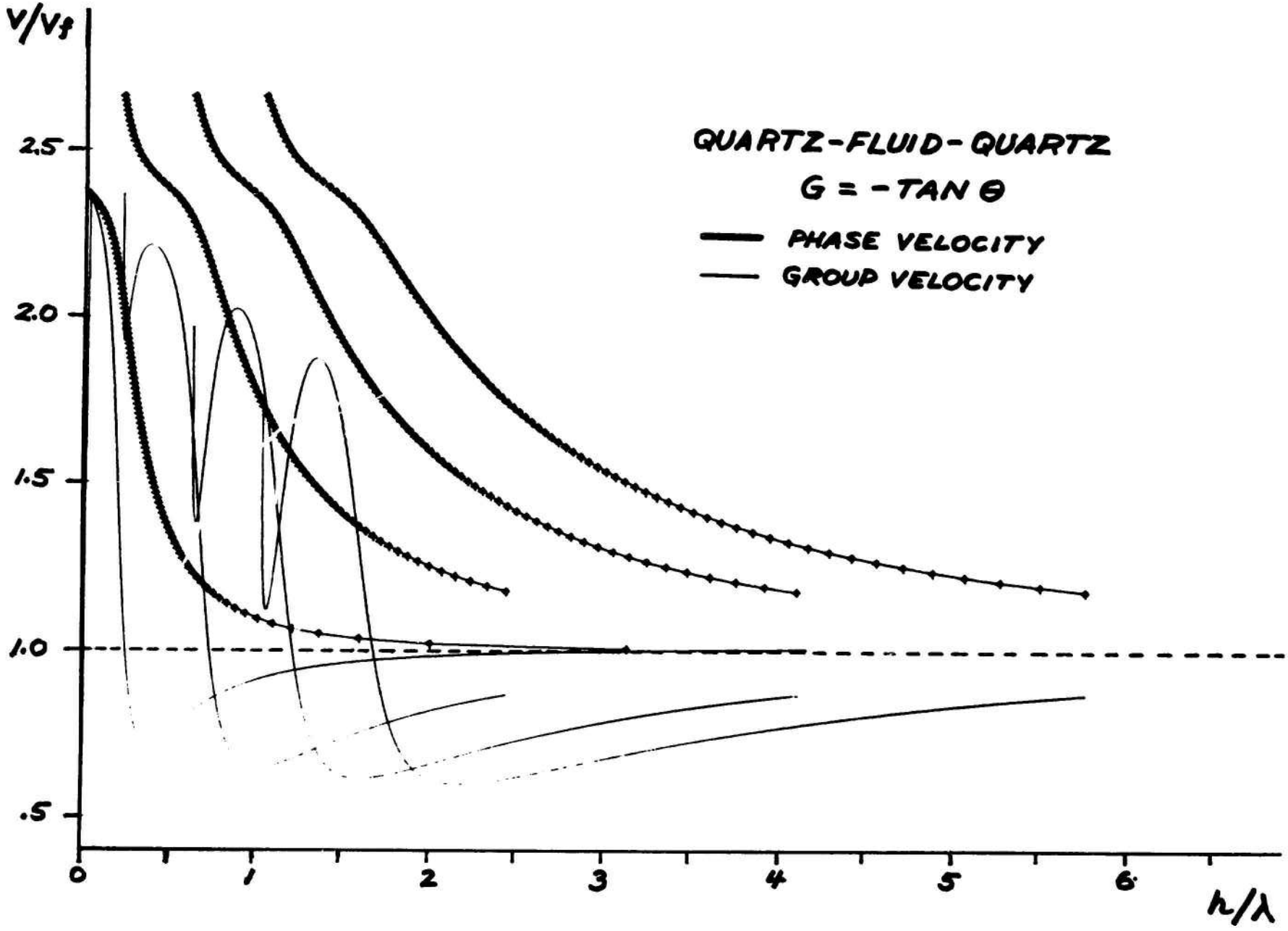
V/Vf
2.5
2.0
1.5
1.0
.5
0
1
2
3
4
5
6
h/λ
QUARTZ-FLUID-QUARTZ
G = -TAN θ
PHASE VELOCITY
GROUP VELOCITY

FIGURE 2b.

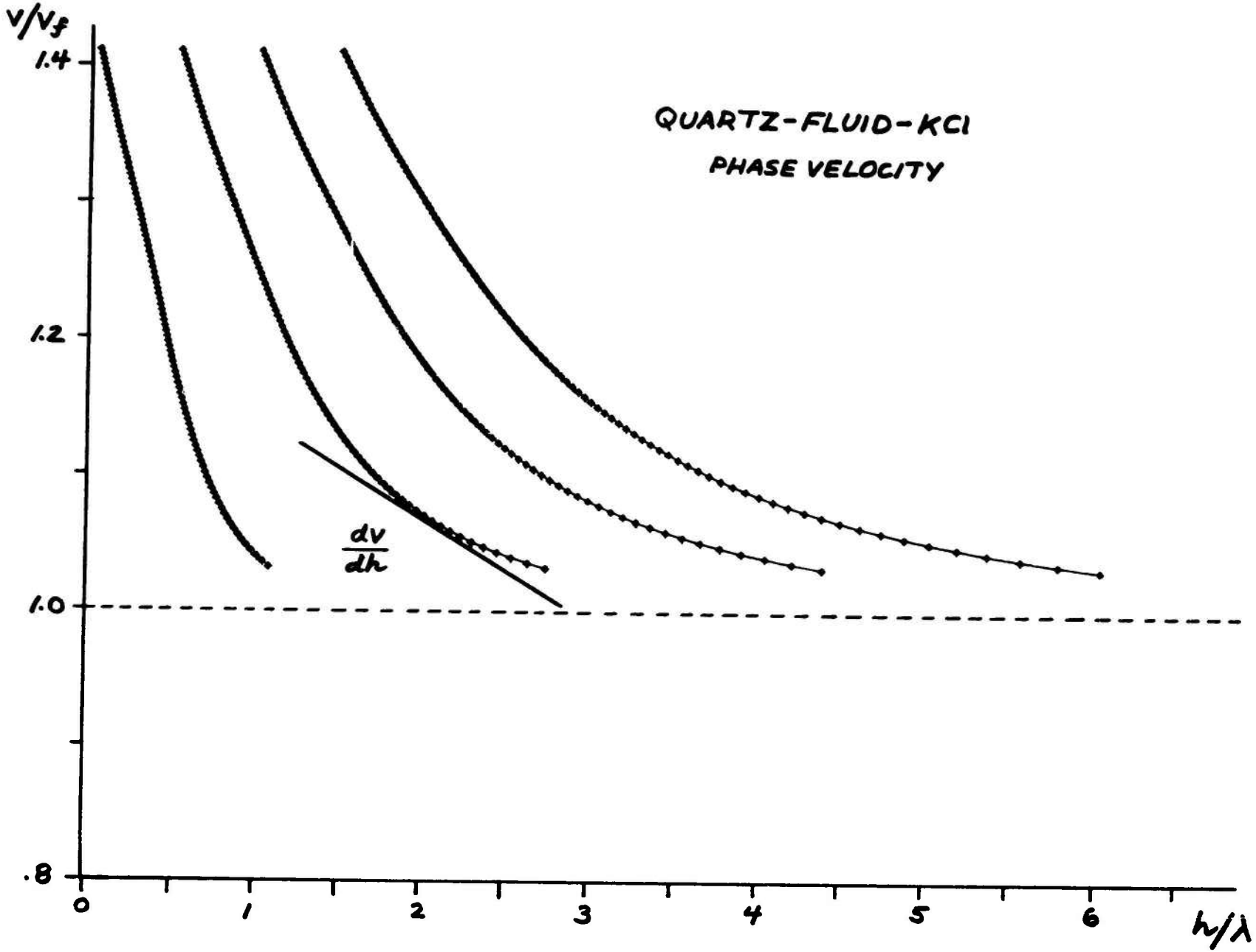
V/Vf
1.4
1.2
1.0
.8
QUARTZ-FLUID-KCl
PHASE VELOCITY
dv/dh
0
1
2
3
4
5
6
h/λ

FIGURE 3a.

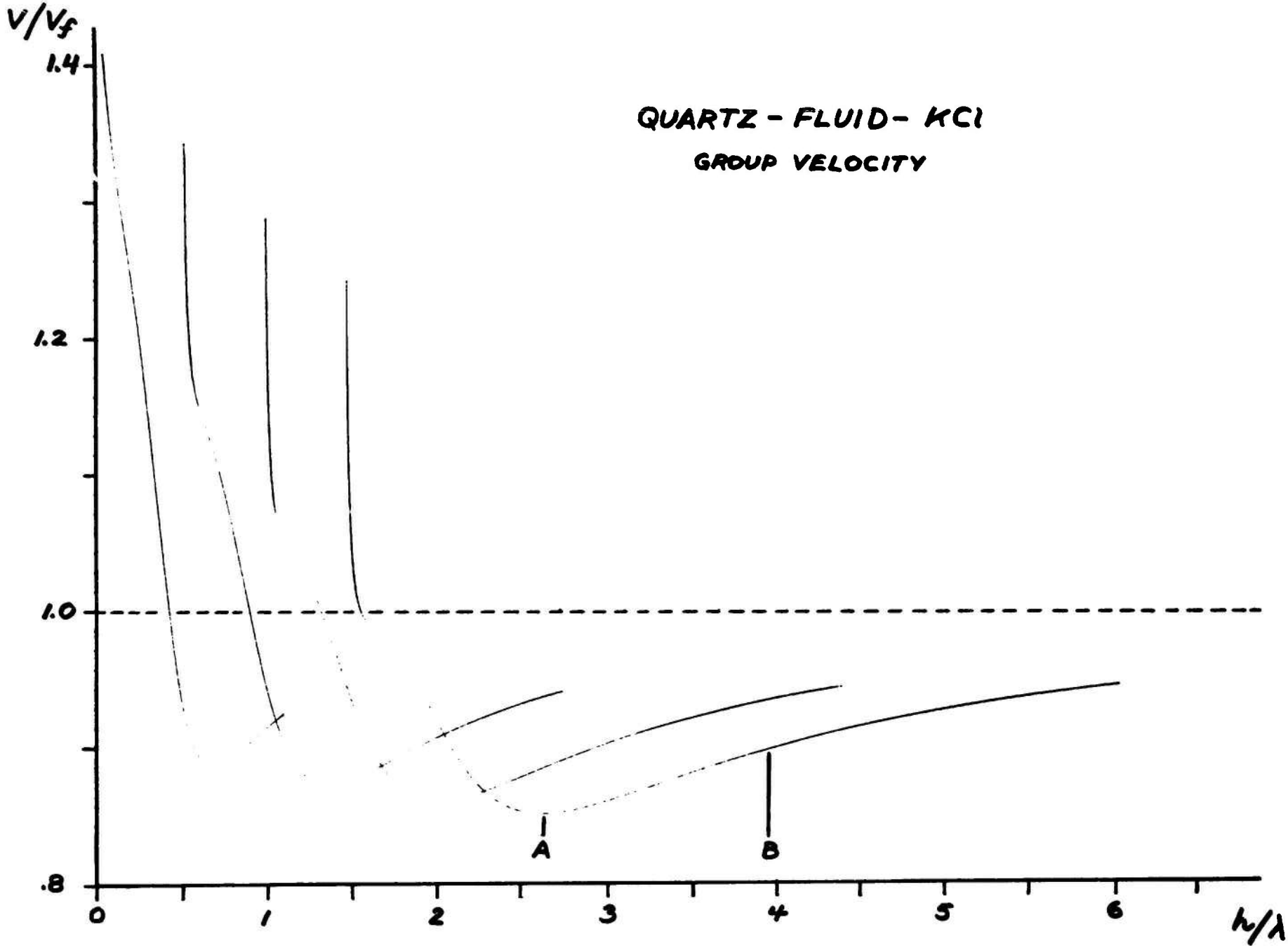

FIGURE 3b.

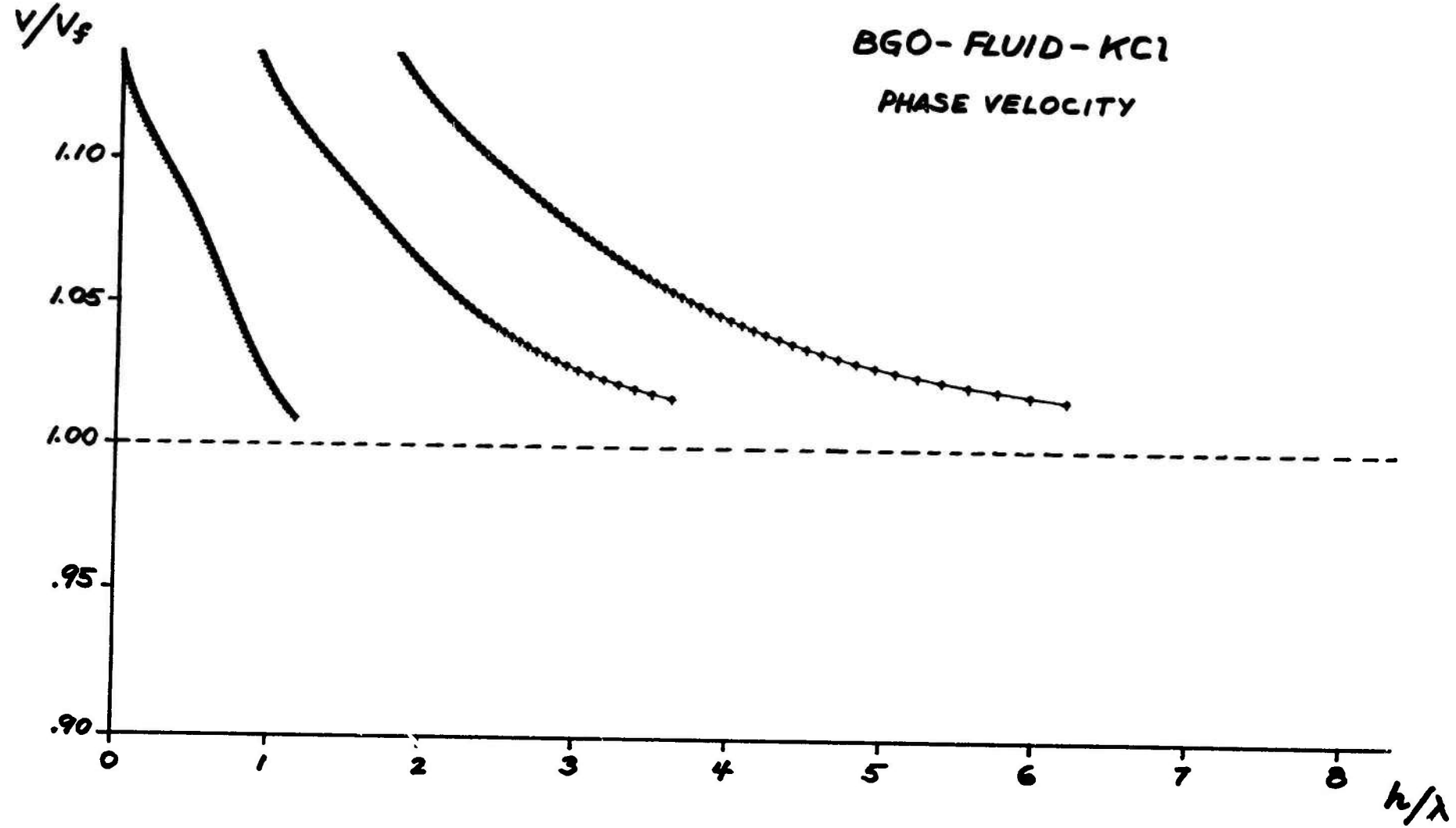
V/Vf
BGO- FLUID - KCl
PHASE VELOCITY
1.10
1.05
1.00
.95
.90
0
1
2
3
4
5
6
7
8
h/λ

FIGURE 4a.

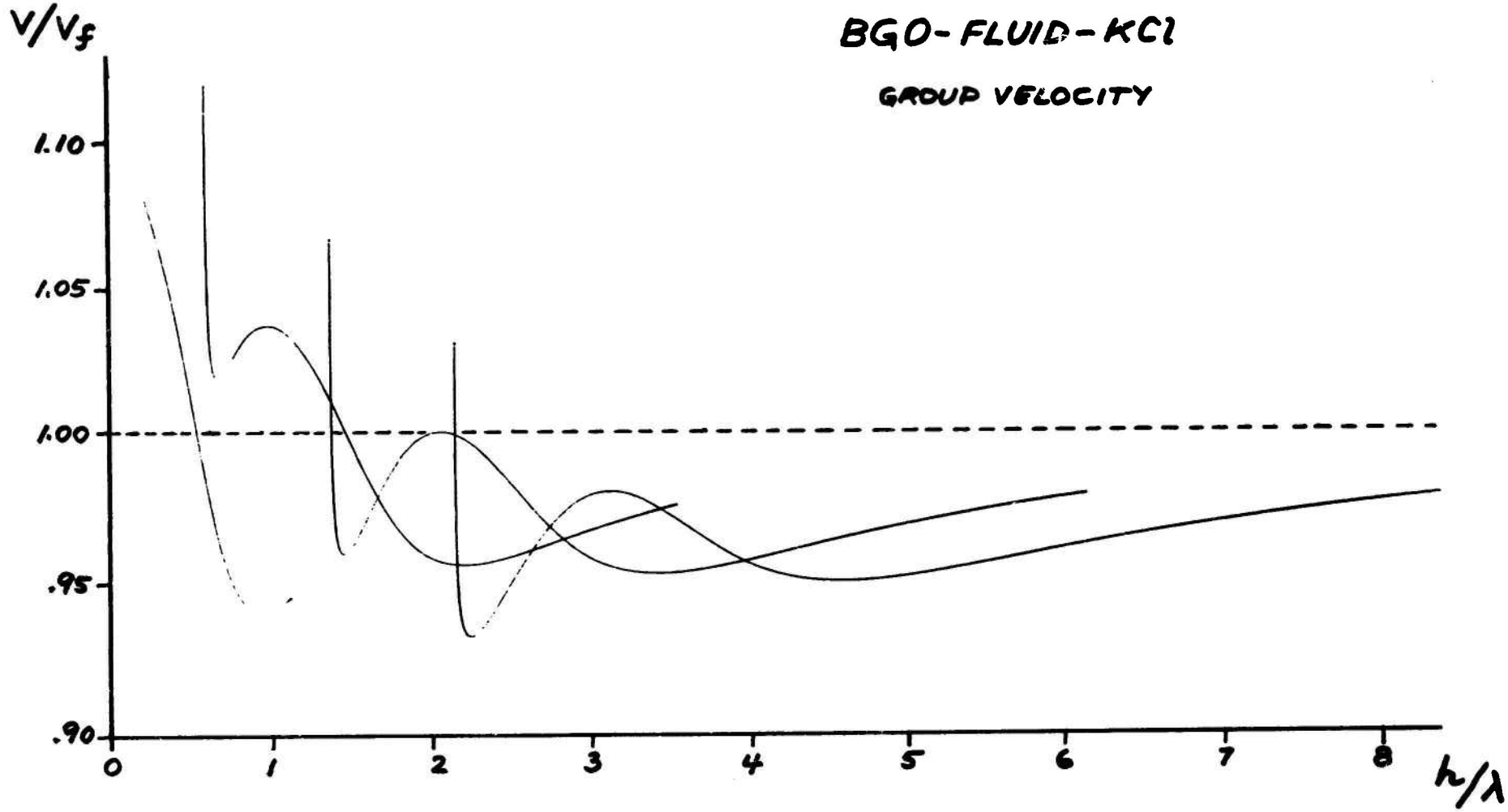
V/Vf
BGO-FLUID-KCl
GROUP VELOCITY
1.10
1.05
1.00
.95
.90
0
1
2
3
4
5
6
7
8
h/λ

FIGURE 4b.

Figure 5. Experimental configuration for surface heat pulse detection showing two arrangements of interdigital transducers and thin film metallic resistor. The acoustic wave of beamwidth 1.25 mm probes the heated region beneath the aluminum thin film resistor.

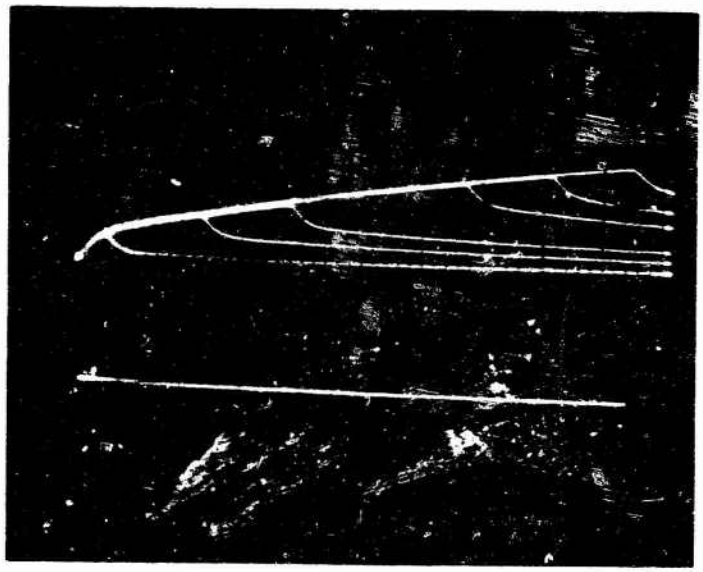

Figure 6a. Resistive heat pulse detection (multiple exposure)

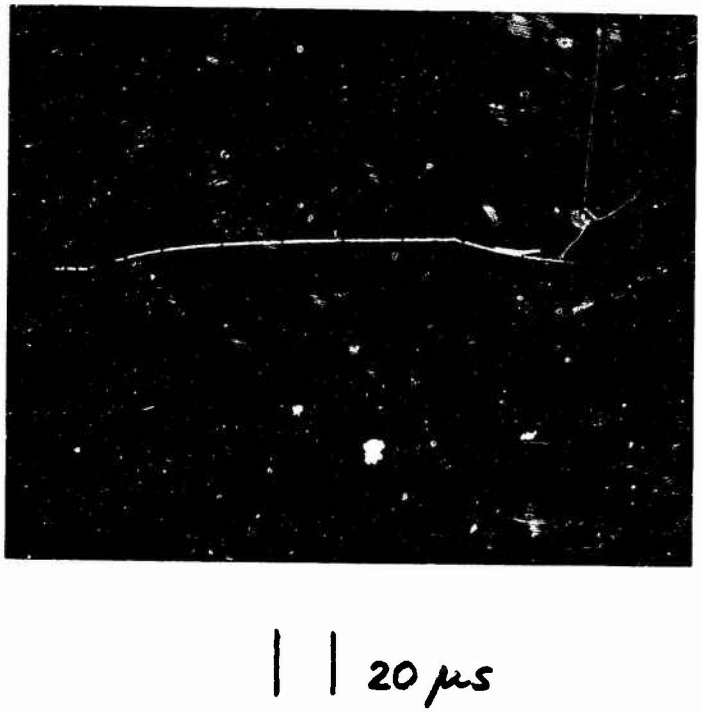

Figure 6b. Resistive heat pulse detection

Y-CUT QUARTZ HEAT DETECTION

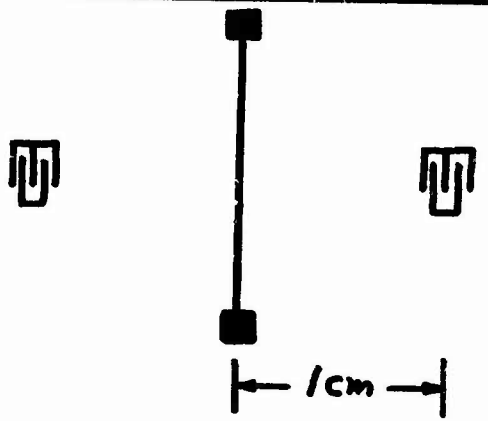

AL RESISTOR ~ 45Ω/mm

$\lambda_s = 25\mu$ $\nu_s = 120$ MHz

BEAM WIDTH ~ 1.25 mm

~3μs TRANSIT TIME

$\tau_p = 1/2\ \mu s$

$P = 24$ w

$E = 12\ \mu J$

$\Delta\phi \sim 1$ mRAD

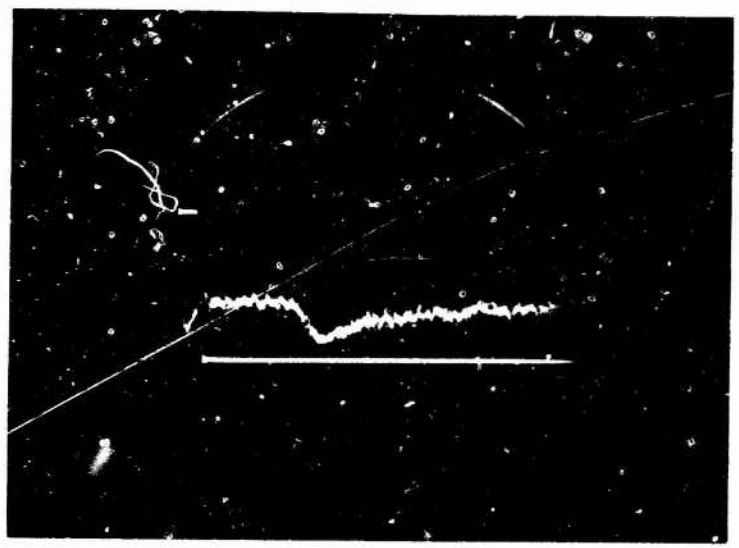

5mv

1μs

FIGURE 7

Y-CUT QUARTZ HEAT DETECTION

AL RESISTOR ~ 4.5Ω/mm , $\lambda_s = 25\mu$ $\nu_s = 120$ MHZ

$\tau_p = .5\,\mu s$
$P = 24\,W$
$E = 12\,\mu J$
$\Delta\phi \sim 1$ mRAD

$\tau_p = 1\,\mu s$
$P = 6\,W$
$E = 6\,\mu J$
$\Delta\phi \sim \frac{1}{2}$ mRAD

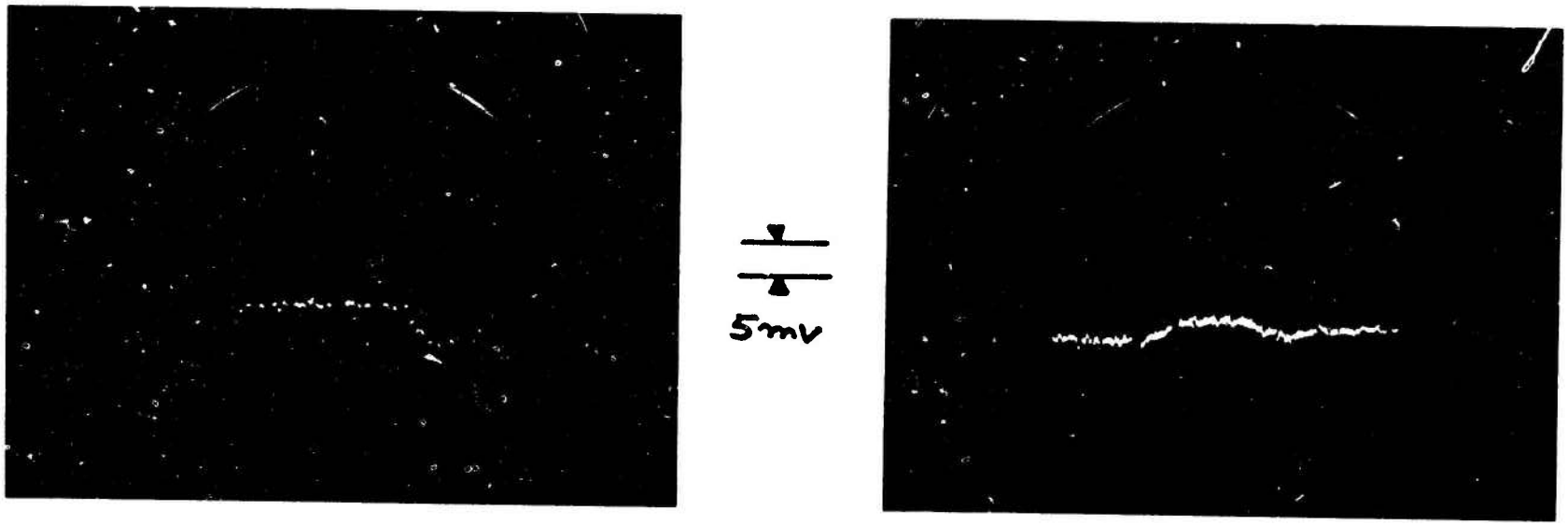

FIGURE 8

1. **Y-CUT QUARTZ**

$$\frac{\Delta\phi}{\phi} \sim (\alpha_L - \alpha_v)$$

$$\sim (13.7 - 40) \times 10^{-6}/^{\circ}C$$

FOR $\tau_p = 16.7$ ms

$$\frac{\Delta\phi}{\phi} \sim -40 \times 10^{-6}/^{\circ}C$$

SLOPE $\Delta\phi/\tau_p \sim .6$

2. **ST CUT QUARTZ**

$\Delta\phi = 0 \quad \alpha_L = \alpha_v = 13.7 \times 10^{-6}/^{\circ}C$

FOR $\tau_p = 16.7$ ms

$$\frac{\Delta\phi}{\phi} \sim -13.7 \times 10^{-6}/^{\circ}C$$

SLOPE $\sim .2$

RATIO OF SLOPES $\approx$ RATIO OF $\alpha_v \approx 3$

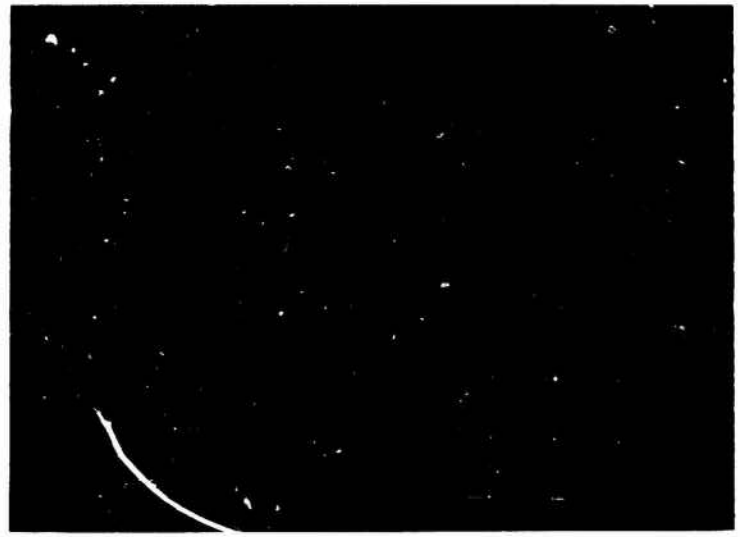

FIGURE 9

g.1 Characterization of Optical Performance of IR Window Systems

Martin Flannery, John H. Marburger

I. Caustic Surface Analysis for Thermal Lensing

a) A ray and caustic surface analysis was performed for a Gaussian beam centered in a circular window in an attempt to explain some of the field patterns from earlier computer runs. For defocusing materials the caustic surface is an axial line plus a parabola-shaped curve extending outward from the focal point. The presence of the axial line seems to account for the fact that the maximum intensity was always found on-axis. It was hoped that the off-axis portion of the caustic surface might define the position of the major off-axis intensity peak, but this is not the case. For small times both caustics lie within the central peak, while for long times the off-axis caustics approximate a small off-axis maximum.

Apparently most of the behavior of the beam is not related directly to the location of the caustics, but is due primarily to crossings of ray bundles from separated areas of the initial wavefront.

b) Some work has also been done on the behavior of a beam of one large central Gaussian and a smaller, slightly off-axis Gaussian. It is easy to show that the central spots of the Gaussians are either spread apart or focused depending on the properties of the window. In particular, for the beam reported in the work of Skolnik et al., it is not hard for the central ray to slew off-axis by a milliradian. However, examination of the rays associated with the 1/e point of the central Gaussian suggests that most of the rays remain nearly on-axis while the rays suffering large amounts of slewing are rather widely scattered.

II. Analysis of Stress Fields in Non-Uniformly Stressed Windows

a) The acentric Gaussian beam described in part Ib is being used in computer calculations including stress birefringence under the assumption that the stress pattern does not include certain acentric edge effects of the off-axis Gaussian. Since an accurate analytic solution for the stresses from an off-axis Gaussian heat source is extremely complex, we have found the exact stresses for an acentric point beam in thermal equilibrium and compared them to the same beam but with the assumption that the stresses are circularly symmetric about the point beam.

The exact analysis predicts lower stresses at the edge nearest the beam than the approximate analysis, but very little change in the direction of the principle stresses. The exact analysis also shows that any slewing of a central beam is slightly less than the approximate theory predicts.

b) The effect of edge loading on the window from its mount may produce rather dramatic effects on the optical output.

The simplest case is uniform radial stresses on the perimeter. The result is a constant radial stress throughout the window which produces no effect on the isotropic window behavior, but will produce increased birefringence.

The second case considered was a knife edge chuck mount with the knife edges under constant pressure. The analysis was for a symmetric three-point chuck, but can be generalized easily to the case of asymmetric chucks. The chuck produces a three-leaf clover pattern in both the isotropic deflection and the birefringence. In general the light will tend to curve towards the points where the knife edges are applied.

Finally, from a practical standpoint, we are most likely to encounter windows mounted in retaining rings that expand much less than the window.

This is a problem in which the boundary is fixed rather than being under a specified stress. If the window is acentrically heated, the stresses on the edges will in general be larger on the window edges closest and farthest from the acentric heat source, than on the intermediate areas. We have an approximate solution for the acentric point beam for this case, but the solution will probably have to be graphed by computer before any general statements can be made.

REFERENCES:

1. Skolnik, L. H., B. Bendow, P. D. Gianino, A. Hordvik and E. F. Cross Conference on High Power Infrared Laser Window Materials, 30, 31 October and 1 November 1972, Bedford, Mass.

3. DISCUSSION

In order to make a final judgment on GaAs we need a)thick crystals grown at temperatures much below the maximum melting point and b)a check on possible oxygen effects on the absorption coefficient. Preliminary work to achieve the former by chemical vapor transport has been completed. A method of oxygen determination has been developed and tested; it can now be applied to the various GaAs crystals for which the absorption was measured.

Pure KBr crystals have been grown; accurate measurements of absorption were so far hindered by the formation of surface layers by reaction with the atmosphere.

In the CdTe program, the first hot-pressing experiments have been done, but not all experimental difficulties have been overcome. The investigation of the defect structure have been completed. The experimental work is largely in agreement with earlier work by de Nobel. The interpretation is somewhat different, however, and therefore the thermodynamic parameters of defect formation are different. The analysis indicates the experimental conditions leading to high-resistivity, closely stoichiometric material. These do in general not correspond to the phase boundary at which hot-pressing is operating. In order to reap the full benefits of hot-pressing in the presence of Cd(ℓ) or Te(ℓ) it may be necessary to look for other ways to achieve high resistivity.

Capacitance measurements as f(frequency) on a contact metal/semi-insulating Cr-doped GaAs lead to an accurate value of the dielectric constant $\varepsilon = 12.4 \pm 0.12$, close to one published figure, but different from several values determined by microwave techniques. The latter are probably unreliable. Measurements in air of absorption of GaAs close to 10.6 μ as f(T) show the effects of free carriers at $T > 250^{\circ}C$ and also irreversible surface effects attributed to oxidation.

Work on the technique of measuring small absorption coefficients of KCl by acoustic surface waves has proceeded. Coupling between the waves and the non-piezo electric bulk was achieved by a fluid layer.

Controlled experiments of acoustic thermal detection were carried out. Resistive surface heat pulses with an energy as small as 12 μJ and pulse width 0.5 μsec could be detected.

Theoretical work in this period includes continuation of the search

for experimental methods to determine whether multi-phonon absorption is affected by non-linear relation between the polarization density and local ionic displacements. Most promising seems the measurement at two temperatures of the spectrum of the imaginary part of the electric susceptibility. A check on the applicability of the Lyddane-Sachs-Teller relation to GaAs was hindered by the wide variation of published dielectric constant values. Withcompletion of Dr. Crowell's measurements in this area it should be possible to arrive at more definite conclusions in the next report.

A caustic surface analysis for thermal lensing was made which showed that the beam behavior is not related directly to the location of the caustics, but is primarily due to crossings of ray bundles from different areas of the initial wave front. The behavior of beams describable in terms of a large central Gaussian and a small off-axis Gaussian shows that some off-axis slewing may be expected for a small fraction of the rays, but these are widely scattered. Stress fields in non-uniformly stressed windows were analyzed more exactly than before; the results remain practically unchanged. Dramatic effects are to be expected for stress due to edge loading resulting from a ring mount.